THE REDUCTION KINETICS OF IRON OXIDE ORE BY METHANE FOR CHEMICAL-LOOPING COMBUSTION

by

Somaye Nasr

Submitted in partial fulfilment of the requirements
for the degree of Master of Applied Science

at

Dalhousie University
Halifax, Nova Scotia
August 2012

DALHOUSIE UNIVERSITY

DEPARTMENT OF PROCESS ENGINEERING AND APPLIED SCIENCE

The undersigned hereby certify that they have read and recommend to the Faculty of Graduate Studies for acceptance a thesis entitled "THE REDUCTION KINETICS OF IRON OXIDE ORE BY METHANE FOR CHEMICAL-LOOPING COMBUSTION" by Somaye Nasr in partial fulfilment of the requirements for the degree of Master of Applied Science.

Dated: 16 August 2012

Co-supervisors: _____

_____

Readers: _____

_____

DALHOUSIE UNIVERSITY

DATE: 16 August 2012

AUTHOR: Somaye Nasr

TITLE: THE REDUCTION KINETICS OF IRON OXIDE ORE BY METHANE FOR CHEMICAL-LOOPING COMBUSTION

DEPARTMENT OR SCHOOL: Department Process Engineering and Applied Science

DEGREE: M.A.Sc CONVOCATION: October YEAR: 2012

_____

Signature of Author

To *my parents* for their endless love.

TABLE OF CONTENTS

LIST OF TABLES

LIST OF FIGURES

LIST OF ABBREVIATIONS USED

CLC	Chemical-looping combustion
CLR	Chemical-looping reforming
CLH	Chemical-looping hydrogen
CCS	Carbon capture and sequestration
EDS	Energy dispersive spectrometer
FCC	Fluid catalytic cracking
ICP-OES	Inductively coupled plasma –optical emission spectroscopy
IPCC	Intergovernmental Panel on Climate Change
k_0	Constant in Arrhenius equation, 1/min
k	Reaction rate constant, 1/min
E	Activation energy, kJ/mol
LNG	Liquefied natural gas
m	Sample mass, g
P	Partial pressure, atm
R	Universal gas constant, J/mol K
R_o	Oxygen transport capacity for the materials
SEM	Scanning electron microscope
t	Time, min
T	Process temperature, ºC
TGA	Thermogravimetric Analysis
XRD	X-ray diffraction
α	Conversion
γ_{CH_4}	Methane yield

Indices

0	Initial

ABSTRACT

Due to increasing atmospheric carbon dioxide (CO_2) concentration, energy sources that release to the atmosphere smaller amounts of CO_2 are of interest. Initially, all the efforts were focused on increasing the system efficiency, now more attention is being paid recently on capturing and sequestering CO_2 from combustion process and eliminating discharge to the atmosphere from the major source points. In these circumstances, the chemical-looping combustion (CLC) is a promising concept that can be used in power generation which integrates power production and CO_2 capture. The aim of this work is to study reaction kinetics of Chemical-Looping Combustion. In order to come up with a suitable reactor design we should have a good knowledge of the reaction kinetics happening in the air and fuel reactor; then, to get such an information as will be mentioned later, reactivity investigation was carried out in thermogravimetric analysis (TGA).

ACKNOWLEDGMENTS

Apart from my efforts and persistence, this dissertation would not have been possible without the guidance and the help of several individuals who in one way or another contributed and extended their valuable assistance in the preparation and completion of this study. It is a pleasure to thank those who made this thesis possible.

First and foremost, my utmost gratitude to Dr. Michael J. Pegg, who financially supported my research and provided his valuable guidance and advice.

I want to show my particular gratitude to my co-supervisor Dr. Kevin Plucknett for his never ending patience and guidance. Without his guidance and persistent help this dissertation would not have been possible. I had the privilege to be a member of his active research group. He always took the time to patiently correct my writing, and I learned a lot from him.

Many thanks to the members of the supervisory committee Dr. Stephen Kuzak and Dr. Dominic Groulx for their valuable time.

Thanks are also due to Patricia Scallion who patiently instructed me how to use the SEM machine and always was there for assistance. I would like to thank Ray Dube, who not only as a lab technician but also as a good friend was always willing to help and give his best suggestions. I will never forget that without his help the experiments would have not finished. Also I would like to thank Dean Grijm, and especial thank to my friend Aminul for helping me with laboratory tasks.

Thanks to my reliable and trustworthy friends back home. I am especially grateful to my close friend, Leila, for her unfailing moral support from afar. She was always there cheering me up and she inspired me greatly to keep trying.

A special thanks to my sisters, Elham, Elahe, and Najme, for your values for everything that they have done for me, they were always supporting me spiritually and encouraging me with their best wishes. I would like to express my deepest appreciations to my parents, Mehri and Reza, for their confidence and unconditional support during my lifetime although they are not here in person I still feel their support and prayer in every single moment.

Last but not the least, the one above all of us, the Omnipresent God, for answering my prayers for giving me the strength to plod on despite my constitution wanting me to give up sometimes, thank you so much my Dear God.

CHAPTER 1 INTRODUCTION

The world climate and the long term impact of climate change have been under critical discussion during the last decade. According to the IPCC (IPCC 2007), " warming of the climate system is unequivocal ". Global warming is a consequence of the increasing emission of greenhouse gases into the earth's atmosphere, primarily due to human activities. CO_2 is arguably the most significant anthropogenic greenhouse gas.

In recent years more concern has risen about CO_2 emission .In addition, continually increasing energy usage leads to increasing requirement in terms of power generation, together with increased emissions of greenhouse gases. As global warming is one of the main topics of concern at the present time, developing new science and technologies for energy supply, which minimizes or eliminates the CO_2 emissions, is an extremely important issue. Capturing CO_2 from flue gases at power stations, or other large point sources, is a good solution to this problem and one of the efficient ways to address this issue.

Among available technologies chemical looping combustion (CLC) has been identified as a promising technology to reduce CO_2 capture cost from power plants. It's an efficient method for CO_2 capturing, as no energy is lost for its separation. In this process a solid oxygen carrier transfers oxygen from the air to the fuel, also acting as a heat transfer medium. The CO_2 can be easily separated through water vapor condensation. The rate of the reaction and the oxygen transfer capacity of the oxygen carrier are of importance in achieving optimal operation. The oxygen carrier also affects the circulation rate of metal oxide in fluidized bed reactors.

Basically, the idea of the chemical looping combustion is that the oxygen needed for fuel combustion is not taken directly from air, but it is supplied by means of an oxygen carrier. Hence air and fuel remain in separate environments and the combustion flue gas mainly consists of steam CO_2 and water vapour, steam is then removed by condensation

and the obtained near pure CO_2 is ready for sequestration in the natural reservoirs undergrounds or in the deep ocean. In the CLC process the NO_x formation is very low by virtue of relatively low temperature in the system.

CLC has attracted extensive interest in recent years; there are still a number of issues that require further investigation. For example, development of oxygen carriers with excellent reactivity and stability is still one of the main challenges for CLC. Construction and operation of large-scale CLC systems is needed before this technology can be applied commercially. As novel techniques of producing synthesis gas and hydrogen using chemical-looping process, chemical-looping reforming (CLR) and chemical-looping hydrogen (CLH) deserve further research in the future.

The main objectives of the present work have been investigating the reduction reaction kinetics by means of the thermogravimetric analyzer (TGA) in an isothermal mode. Utilizing iron ore pellets for the CLC process has been studied. The results of the experiments prove the iron ore to be a good candidate for this process. The obtained results could be employed in the fuel reactor design. In the following thesis, Chapter 2 covers an initial background on the CLC process and reduction reaction studies, while the experimental process is presented in Chapter 3. Chapter 4 covers the results and discussion on the obtained experimental work. The conclusions and some recommendations for future work are then outlined in Chapter 5.

CHAPTER 2 CO_2 CAPTURE

2.1 CO_2 Capture and Storage (CCS)

The CO_2 capture and storage technologies are used to extract a stream of CO_2 from gas streams emitted from industrial plants, transport it to a storage location and ultimately store it away in from the atmosphere in an underground reservoir for a long period of time; thus it will not contribute to the greenhouse effect anymore.

The Intergovernmental Panel on Climate Change (IPCC) report on carbon dioxide capture and storage (2005) provides an overview of the alternatives for the capture, transport and storage process. Among three steps of CCS (capture, transport and storage), CO_2 capture is the most costly one. It could be concluded that CO_2 capture has a crucial influence on reducing the process cost. At present, there are three approaches to achieve CO_2 capture from power plants:

- Pre-combustion decarbonization
- Oxy-fuel combustion
- Post-combustion CO_2 capture

All three options are energy-intensive. For pre-combustion decarbonization, carbon must be removed from the fuel, while for the oxy-fuel process oxygen needs to be separated from the air, and for post-combustion capture CO_2 must be stripped off, and it is then diluted with other gases in the power plant exhaust. The use of the above technologies will result in efficiency reductions, thereby leading to increased energy prices. Chemical-looping combustion on the other hand, separates CO_2 inherently by using an oxygen carrier and can ultimately prove to be a technology for highly efficient power generation with CO_2 capture, and consequently it is one of the most promising alternate concepts. Since CO_2 cannot be eradicated completely, its emission can be potentially reduced to an acceptable level using CLC technology. A brief review of these technologies can be found in the work of Toftegaard et al. (2010).

2.2 Chemical-Looping Combustion (CLC)

Chemical-looping combustion (CLC) has emerged as a novel combustion technology for CO_2 capture from fossil fuel combustion in power plants. The CLC process was originally used to increase thermal efficiency in power generation stations, but subsequently its advantages for effective CO_2 separation were discovered (Ishida et al., 1987; Richter & Knoche, 1983). CLC also has possible applications in the oil and gas industry, in order to replace conventional CO_2 capture systems in heaters and boilers.

Despite conventional combustion, in the CLC the fuel is not in direct contact with air and the combustion takes place in two reactors. Air and fuel are kept away from each other in these separate reactors. The required oxygen is supplied by a metal oxide, which is referred to as an 'oxygen carrier'. One of the main drawbacks of the conventional combustion is that a large amount of energy is needed to separate and collect CO_2 from the exhaust gas in the traditional combustion process, because CO_2 is diluted by N_2 from the combustion air.

A typical CLC unit, shown schematically in Figure 2.1, consists of two main reactors, an air and a fuel reactor, with a metal oxide (Me_xO_y ,Me_xO_{y-1}) as an oxygen carrier medium. In the fuel reactor, the oxygen carrier is reduced through oxidation of the fuel; following Reaction (2.1) and (2.2) take place in the air reactor, where the oxygen carrier is regenerated, as the inlet air flow reacts with the solid oxygen career. The net chemical reaction is the same as usual combustion method, with the same heat of combustion released.

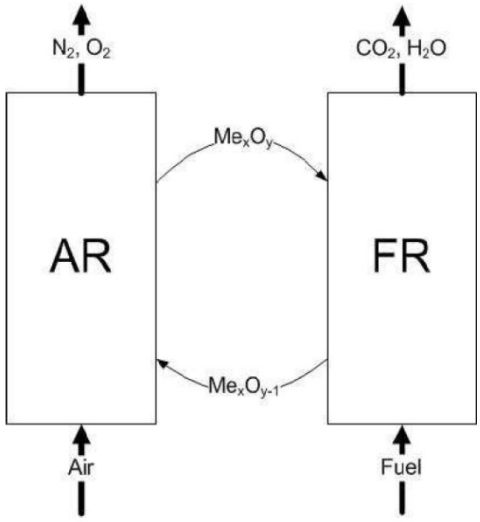

Figure 2.1 Schematic description of chemical-looping combustion AR (air reactor), FR (fuel reactor)

2.3 Chemical Reactions in the CLC Process

Reactions in the CLC process are quite simple because the process is based on oxidation and reduction. The reactions are gas-solid reactions where fuel and air refer to gas and particles refer to solid phase. The following reactions occur on the surface of the particles; thus the greater surface area the more efficiently the reaction would proceed.

Reduction in the fuel reactor:

$$mMeO + C_nH_{2n+2} \rightarrow mMe + (n+1)H_2O + nCO_2 \quad (2.1)$$

Oxidation in the air reactor:

$$mMe + \frac{m}{2}O_2 \rightarrow mMeO \quad (2.2)$$

Net reaction:

$$C_nH_{2n+2} + \left(\frac{3n+1}{2}\right)O_2 \rightarrow (n+1)H_2O + nCO_2 \quad (2.3)$$

Here MeO is the fully oxidized oxygen carrier and Me is the oxygen carrier in the reduced form.

The oxidation reaction is exothermic, while the reduction reaction can be either endothermic or exothermic, depending on the metal oxide used. The amount of released energy released from each reaction depends on the metal oxide and fuel that was used.

A solid oxygen carrier (metal oxide) is used to transfer the oxygen from the air to the fuel. The oxygen carrier circulates between the air reactor, where it is oxidized by the air (Equation 2.2), and the fuel reactor, where it is reduced by the fuel (Equation 2.1). Hence, the air is not mixed with the fuel, and the CO_2 is not diluted by the N_2 in the air. The outgoing gas from the oxidation step will contain N_2 and unreacted O_2, while the gas from the reduction step will be a mixture of CO_2 and water vapour. The water vapour can be condensed, and close to pure CO_2 is then obtained. Some additional energy input is still needed to compress the CO_2 into a liquid form, suitable for transportation and storage (Lyngfelt et al., 2001).

As mentioned earlier, depending upon the metal oxide used, the reduction reaction is often endothermic ($\Delta H_{red} > 0$), while the oxidation reaction is highly exothermic ($\Delta H_{oxd} < 0$). The total amount of released heat, ΔH_c, is the same as for normal combustion.

$$\Delta H_c = \Delta H_{red} + \Delta H_{oxd} < 0 \qquad (2.4)$$

Where ΔH_c is the heat of combustion, ΔH_{red} is the heat of reduction and ΔH_{oxd} is the heat of oxidation reaction.

The CLC also minimizes the formation of thermal NO_x, because the combustion environment in the fuel reactor is air-free, and the reaction temperature (< 1200 ºC) in the air reactor is below the temperature (> 1500 ºC) at which NO_x begin to form. Reactions and oxygen transport capacity (R_o) (Equation 2.12) of selected metal oxides are presented in Table 2.1. R_o is a property of the oxygen carrier, which signifies the mass fraction of oxygen in the carrier.

Table 2.1 Reactions of the metal oxides used in CLC, oxygen transport capacity for the materials, R_o, and the associated heat of the combustion under standard conditions (i.e. 298.15 K and 0.1 MPa) (Abad et al., 2007).

MeO/Me		R_o	ΔH_c° kJ/mol
CuO/Cu			
	CH_4+4 CuO → 4Cu+CO_2+ 2H_2O	0.2	-178.0
	H_2+ CuO → Cu+H_2O		-85.8
	CO+ CuO → Cu+ CO		-126.9
	O_2+ 2Cu → 2CuO		-312.1
NiO/Ni			
	CH_4+4NiO → 4Ni+CO_2+2H_2O	0.21	156.5
	H_2+NiO → Ni+H $_2$O		-2.1
	CO+NiO → Ni+CO_2		-43.3
	O_2+ 2Ni→ 2NiO		-479.4
Fe_2O_3/Fe_3O_4			
	CH_4+ 12 Fe_2O_3 → 8Fe_3O_4 +CO_2+2H_2O	0.03	141.6
	H_2+ 3Fe_2O_3 → 2Fe_3O_4+H_2O		-5.8
	CO+ 3Fe_2O_3 → 2Fe_3O_4+ CO_2		-47.0
	O_2+4Fe_3O_4→ 6Fe_2O_3		-471.9
Others			
	CH_4+ 2 O_2 → CO_2+2H_2O		-802.3
	H_2+ 0.5O_2 → H_2O		-241.8
	CO+ 0.5O_2 → CO_2		-282.9

Due to the ever increasing concerns of CO_2 emissions and the need to develop a long-term solution for this problem at the beginning of the 21st century, the CLC concept has captured much attention in many parts of the world. A research group that focused recent efforts on the CLC concept is the one headed by Anders Lyngfelt at Chalmers University of Technology, Sweden. This group can be designated as one of the largest contributor to the experimental data on the oxygen carriers required in the CLC process. Their early

studies (Lyngfelt et al., 2001) focused on iron oxide (Fe_2O_3, hematite), mainly because it is an inexpensive substance and also due to promising results.

There are other research groups assessing this area (e.g. Lee et al., Garcia- Labiano et al., Adanez et al., Ryu et al., Jeong et al., Corbella et al., Song et al., Villa et al. and Copeland et al.). All of the groups have contributed to the oxygen carrier development. Copeland et al. (2001) came up with a different approach, which is quite similar to the CLC process and focuses on CuO as the metal oxide. The reason for this is that both the reduction and oxidation reactions of CuO are exothermic.

Oxygen carriers play a vital role in the performance of the CLC process. For example, the amount of bed material that is present in both reactors, and the circulation rate of solids between these reactors, is mainly dependent on the characteristics of the chosen oxygen carrier. The metal oxide used as an oxygen carrier should have the following features (Lyngfelt et al., 2001; Hossain & Lasa, 2008):

- Sufficient rates of oxidation and reduction
- Adequate durability in successive cycle reactions under high temperature
- Enough mechanical strength to limit particle breakage, attrition and wear
- Resistance against carbon deposition
- Resistance to agglomeration
- Environmentally safe
- Technically and economically feasible.

Ideally, the number of reaction cycles of the oxygen carrier would be infinite. However, in reality reactivity loss happens during the cycles. In addition, because of mechanical wear, the carrier particles must be replaced periodically.
In general, suitable metal oxides are combined with an inert which acts as a porous support, providing a higher surface area for reaction, as well as better mechanical strength and attrition resistance. In Figure 2.2 the shape and surface structure of a Mn-based oxygen carrier, supported with zirconia, can be seen.

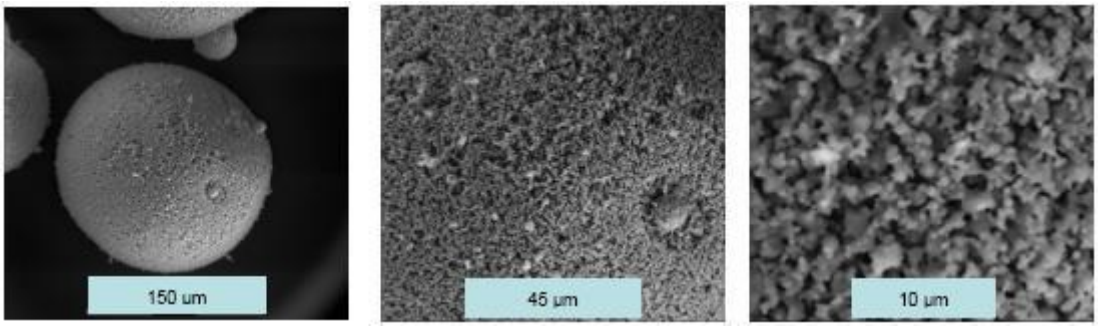

Figure 2.2 Oxygen carrier composed of 40 % Mn_3O_4 on 60 % partially stabilized zirconia (Mg-ZrO_2) (Mattisson et al., 2006).

The fuel and air mass flows, thus the air to fuel ratio, are determined by the desired power output. The most crucial input data is the type of the oxygen carrier. A considerable amount of work has been done to find the best possible metal oxide/inert support combination. Because of mechanical wear and reactivity loss during the cycles, carrier particles must be replaced periodically. The regeneration of the metal oxide is highly exothermic and design allowance must be considered to account for the possibility of high-temperature excursions, in order to avoid thermal sintering of the carrier (Ion Iliuta et al., 2010)

2.4 Reactor

Up to 2001, most of the research work on CLC focused on the development of various oxygen carriers. However, there is not much information published about how the CLC reactors should actually be designed. In the CLC process a good contact between the fuel and oxygen carrier, along with a flow of solid material between the two reactors, is required.

Reactor design of a CLC combustor must be done carefully. Intimate contact between the oxygen carrier and the gas phase is important, in order to obtain high performance. Phase contact is strongly related to the reactor configuration. A suitable reactor system in a combined cycle has to meet the following requirements (Wolf, 2004):

- Adequate particle transport between reactors
- Provide a sufficient reaction time for the reactions
- Prevent gas exchange between reactors
- Reach a high temperature in the outlet of the reactor
- Withstand the required pressure

2.4.1 Characterization of CLC Reactor Systems

The two reactors involved in the CLC process are different types regarding their operation, and must meet certain requirements depending on the nature of the gases and the reactions. A very high degree of fuel conversion should ideally be achieved in the reduction reactor so that it can be assured that the exhaust stream is pure and is comprised of CO_2 and water vapor. The rate of oxidation also must be high enough to transfer heat to large amounts of air in the oxidation reactor.

2.4.1.1 Fluidized Beds

The solids circulation in CLC is like that taking place in the process of fluid catalytic cracking (FCC), which is a widely used conversion process in petroleum refineries. CLC differs from FCC in that the CLC oxygen carriers undergo chemical reactions, while the FCC solid components act as catalysts. In general, fluidized beds have several appealing advantages for an application such as CLC. One of the most important advantages of a fluidized bed is an outstanding gas-solid heat and mass transfer.

Another advantage of fluidized bed is the 'liquid-like' behavior of the fluidized solids, thereby simplifying the handling of large amounts of solids within the system. Moreover, the oxygen carrier inside the reactor provides a thermal reservoir that prevents any rapid temperature changes, thus it maintains a stable temperature for the gases leaving the reactors. This is an advantageous aspect in terms of stable reactor operation. One of the drawbacks of such a reactor is the problem associated with the erosion of the pipes. There may also be high particle attrition rates.

Lyngfelt et al. (2001) proposed a recirculating system composed of two connected fluidized beds, with a high velocity riser as an air reactor and a low velocity bubbling bed as a fuel reactor (Figure 2.3). The solid particles leaving the riser are recovered by a cyclone and sent to the fuel reactor. The fuel reactor is located at a relatively high level, thus the reduced particles are returned to the air reactor by means of gravity.

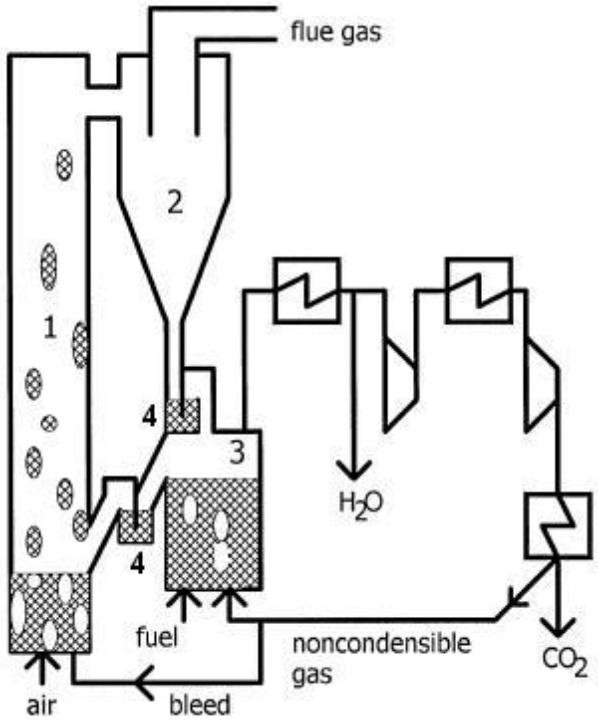

Figure 2.3 Chemical-looping combustion reactor layout: (1) Air reactor, (2) cyclone, (3) fuel reactor, and (4) particle lock (Lyngfelt et al., 2001).

In a configuration of interconnected fluidized beds like that shown in Figure 2.3, the possibility of gas leakage must be minimized. Fuel gas leakage from the fuel reactor to the riser results in CO_2 release into the atmosphere, which reduces the efficiency of the carbon capture process. Air leakage from the riser to the fuel reactor dilutes the combustion gas with N_2, which adds extra costs to CO_2 separation. Leakage between the reactors can be reduced with two gas locks, one placed between the cyclone and the fuel reactor, and the other between the fuel reactor and the riser (Lyngfelt et al., 2001).

Flue gas from the fuel reactor contains mainly CO_2 and H_2O, but there can also be a minor amount of unreacted fuel, such as methane. After condensation of the water, the remaining gas is compressed and cooled to yield liquid CO_2, while the non-condensable fuel gas is recycled back to the fuel reactor. Some part of this flow is bled to the air reactor, in order to avoid accumulation of non-combustible gases, like N_2 (Lyngfelt et al., 2001).

The volumetric gas flow in the riser is approximately ten times larger than that of the gaseous fuel in the fuel reactor. High gas velocity is chosen in the air reactor in order to retain a moderate size for the reactors. An oxidation reaction is usually much faster than a reduction reaction (Yan Cao et al. 2004); as a consequence it is easier to size an air reactor than a fuel reactor. Full conversion of the oxygen carrier should be considered in the reactor design. In addition to the higher gas velocity, an air reactor also has a higher pressure and temperature than a fuel reactor.

The major drawbacks of fluidized bed reactors are:

- Pressure drop
- Erosion of pipes
- High particle attrition rates

2.4.1.2 Packed Bed Reactors

The main advantage of a packed bed reactor is that the separation of gas and particles is intrinsically avoided, so that the reactor can be more compact. In comparison to fluidized bed reactors, a large difference in the degree of oxidation can be obtained between the reduced and oxidized forms of the oxygen carrier (Noorman, 2010)

For continuous operation, two beds are required; one is for oxidation while the other is for the reduction step. In between the two reactions a purge step should be used in order to:

- Avoid formation of explosive mixtures

- Equalize the temperature profiles
- Better use the evolved heat during the oxidation step

2.4.1.3 Rotating Bed CLC Reactor

CLC is a cyclic process in which fuel is burnt by a metal oxide. After combustion the reduced metal oxide is re-oxidized in an air reactor to be prepared for a new cycle. Such a reduction-oxidation, or redox, cycle can be done in two ways; either by moving the metal oxide between 'static' gas streams or keeping the metal oxide static while switching the gas streams.

The first option is implemented by a circulating fluidized bed (CFB) arrangement, in which the metal oxide powder circulates between the fuel reactor, where combustion takes place, and an air reactor, where re-oxidation is carried out. The second option involves one or more fixed bed reactors, where complex valving ensures cyclic gas feeds to the reactors and optimal gas separation.

The rotating CLC reactor system, is shown schematically in Figure 2.4. An alternative is the rotating CLC-reactor system resembling the 'CO_2 wheel' proposed by Shimomura [2003]. Metal oxide is kept in a doughnut shaped fixed bed reactor that rotates between different gas streams flowing radially outward through the bed. Radial gas flow is a good choice for a CLC process due to gas expansion. However, a major drawback of the rotating reactor configuration is gas mixing. The rotary CLC reactor concept is currently in the early phase of research and concept development at Alstom (Jukkola et al., 2003).

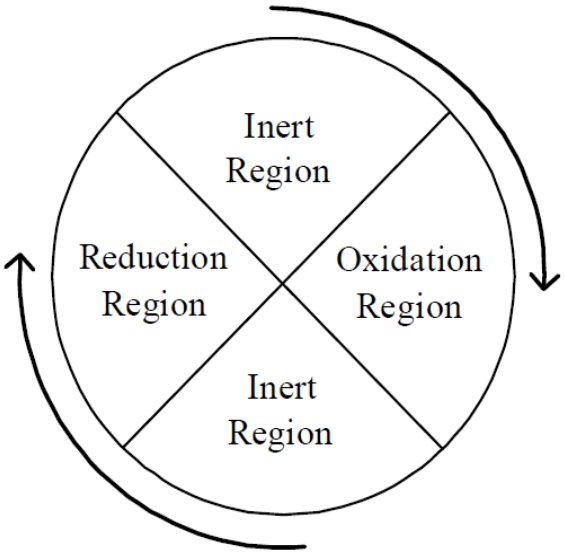

Figure 2.4 Rotary CLC reactor schematic

2.5 Design procedure for a CLC system

Kronberger et al. (2005) suggested a design procedure for CLC processes for the specific case of fluidized bed reactors. Desired power output, reaction kinetics, hydrodynamics, mass and heat balances, and reactor geometry, which are determined by the design input data, desired power output, chosen oxygen carrier, and fuel type, are all considered in that the suggested approach. Figure 2.5 shows how different design specifications and operational features are linked together in this procedure.

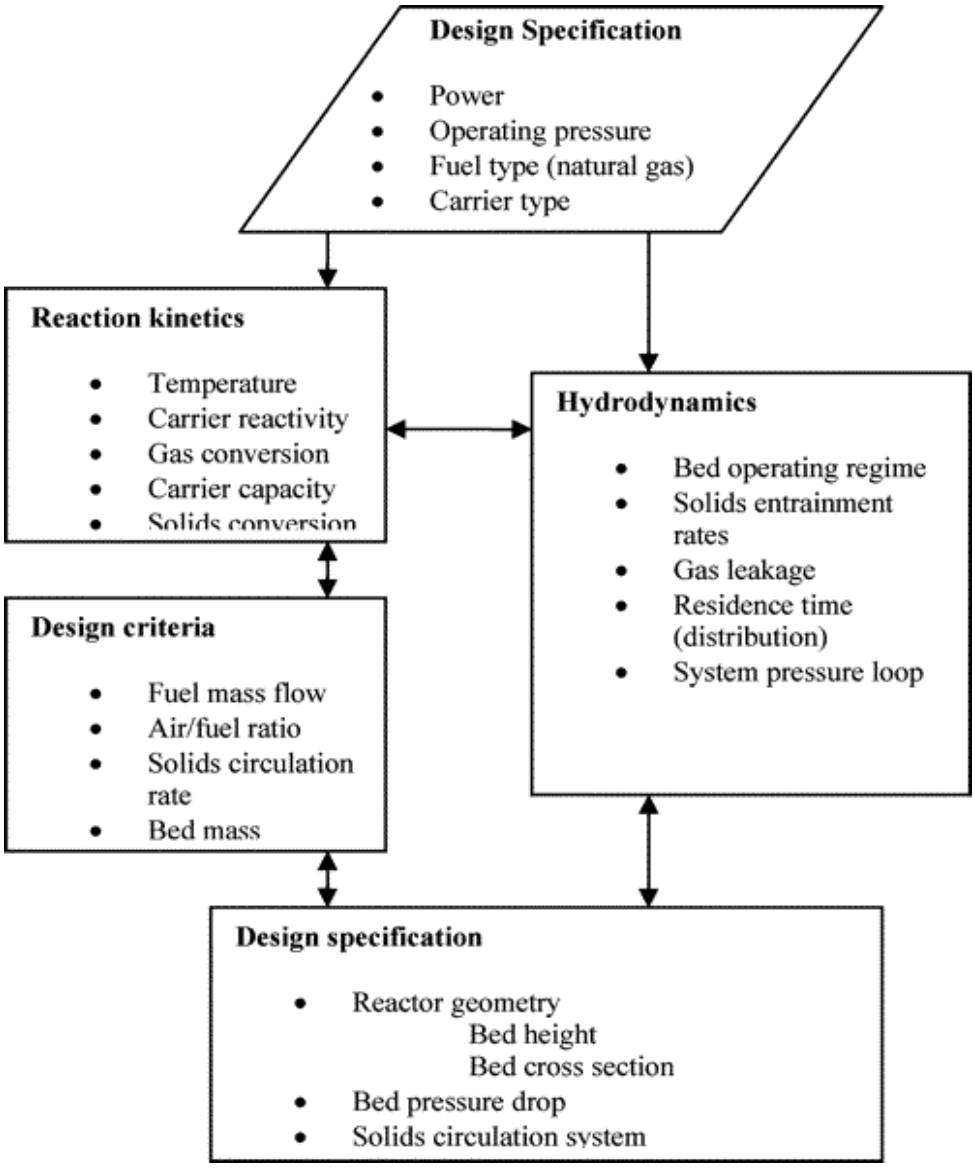

Figure 2.5 Design procedure for a CLC fluidized bed system (Kronberger et al., 2005).

2.6 Mass and heat balances

The air and fuel mass flows are determined by the desired power output. The most important input data is the type of oxygen carrier. It determines both the circulation rate of solids between reactors and the amount of bed material required in the two reactors. The circulation rate must be high enough to transfer the required amount of oxygen needed for fuel combustion. The amount of bed material in the two reactors must be

adequate to have sufficient conversion of reaction. A high reaction rate means a smaller bed mass is needed.

2.7 Fuels

Most of the work that has been done on the CLC processing in the last decade has focused on natural gas as a fuel. It would be highly advantageous if the CLC process could be adapted for coal combustion, as there are vast coal resources available and it is less expensive than natural gas, although it is difficult to reach complete conversion with solid fuel. Using syngas as fuel in the CLC process would be an alternative way to have an economical process in future.

2.7.1 Combustion of Methane

The liquefied natural gas (LNG) fueled power generation system with the CLC combustor arrangement has the following advantages:

1. The CLC combustor does not need pure oxygen; O_2 generation requires high power consumption.

2. Since the reduction reaction produces only carbon dioxide and water vapor, then CO_2 can be easily separated and collected by cooling the exhaust gas.

3. There is no NO_x emission as the oxidation is a gas-solid reaction between a metal and air.

Natural gas contains a high fraction of methane. The reduction reaction between methane and the oxygen carrier is:

$$CH_4 + 4\,MeO \rightarrow CO_2 + 2H_2O + 4Me \qquad (2.5)$$

Depending upon the metal oxide used, the reduction reaction is often endothermic ($\Delta H_{red} > 0$). Although the investigations have shown that the reduction reactivity is faster with syngas (CO, H_2) than methane, when used as a fuel, it is a suitable fuel for a first application of the process (Johansson 2007).

In the CLC process, converting a high fraction of the incoming fuel to CO_2 and H_2O is of interest. Jerndal et al. (2006) studied the degree of methane conversion to CO_2 and H_2O with different types of oxygen carriers. The degree of fuel conversion, or 'gas yield', was defined as the fraction of the fuel which is oxidized to CO_2 and can be obtained by the following equation:

$$\gamma_{CH_4} = \frac{P_{CO_2}}{(P_{CH_4} + P_{CO_2} + P_{CO})} \tag{2.6}$$

Here P_i is the partial pressure of species in the product gas. Table 2.2 shows the measured methane yields with different oxygen carriers and, it shows that complete fuel conversion could be achieved with carriers based on Cu, Fe and Mn.

Table 2.2 Measured methane yields at atmospheric pressure (Mattisson et al., 2006)

	γ_{CH_4}	
	800 ºC	**1000 ºC**
NiO/Ni	0.9949	0.9883
CuO/Cu	1.0000	1.0000
Fe_2O_3/Fe_3O_4	1.0000	1.0000
Cdo/Cd	0.9888	0.9827
Mn_2O_3/Mn_3O_4	1.0000	1.0000
CoO/Co	0.9691	0.9299
Zno/Zn	0.0022	0.0124
$SrSO_4/SrS$	0.9875	0.9738

2.7.2 Combustion of Solid Fuels

Using solid fuels in the CLC process presents some technical problems, such as the separation of the oxygen carrier from the fuel and ash, the possible interaction between the fuel, ash, and oxygen carriers, and the combustion of unburned carbon particles in the oxidizer due to the circulation of solid fuel particles (Yan Cao et al. 2006). There are two ways to perform CLC with solid fuels. The first is to use syngas from coal gasification. This gas, consisting mainly of CO and H_2, can be burned in the CLC process. The gasification needs to be done with O_2 in order to obtain undiluted syngas, and then an air separation unit would be needed. The gasification reaction is slow compared to the reaction between the gasified components and the metal oxide particles. Then, gasification is the rate limiting step of the process (Leion et al., 2007). In comparison to natural gas as a fuel, the oxygen carriers are more reactive with CO and H_2 or a mixture of these, such as syngas (Johansson, 2007). The main gasification reactions are:

$$C + H_2O \rightarrow CO + H_2 \quad (2.7)$$

$$CO + H_2O \rightarrow CO_2 + H_2 \quad (2.8)$$

$$C + CO_2 \rightarrow 2CO \quad (2.9)$$

Another option is to introduce the solid fuel directly into the fuel reactor, where the gasification of the coal will take place. The potential for a solid-solid reaction between the coal and the metal oxide can be problematic, as it is not very likely to occur at any reasonable rate. Compared to gaseous fuels, using solid fuels presents many challenges to the CLC process and the use of solid fuels will require more advanced reactor design (Johanasson, 2007).

2.8 Carbon Deposition

If a hydrocarbon fuel (e.g. methane) is exposed to a high temperature, carbon may form through a number of reactions. Hence, avoiding carbon formation in the fuel reactor of a CLC unit is important. The carbon deposited on the oxygen-carrier in the fuel-reactor can

flow with the particles to the air-reactor and be burnt by air. Therefore, carbon deposition on the oxygen-carrier particles reduces the efficiency of the CO_2 capture and should be avoided.

Carbon deposition is a possible side reaction in the fuel reactor.

Boudouard	$2CO \leftrightarrow C + CO_2$	(2.10)
Pyrolysis	$C_nO_{2n+2} \leftrightarrow nC + (n+1)\,H_2$	(2.11)

Carbon can attach to the particle surface and is then oxidized in the air reactor. Taking into account Equation 2.2, this would decrease the carbon capture efficiency.

2.9 Reactivity and Oxygen Ratio

The reactivity of the oxygen carriers in both oxidation and reduction cycles is an important factor to be considered in the design of a CLC process, because it is related to the solids inventory in the system. The bed mass in the real system is inversely proportional to the reaction rate of the oxygen carriers, so a higher reaction rate means a smaller bed mass required, therefore leading to smaller reactor sizes and lower production costs.

The carrier must be reactive enough to fully convert the fuel gas in the fuel reactor, and to be re-oxidized in the air reactor. Fe, Cu and Ni are the best oxygen carrier candidates because of favorable thermodynamics, high availability and low cost.

The porosity of the particles is increased with the addition of inert fillers and, due to that, the oxidation and reduction rates of the oxygen carrier will be higher. Inert filler incorporation also helps to maintain the structure and increase the ionic conductivity of the particle. The melting point of the oxygen carrier should be high enough to withstand the CLC reaction temperature and avoid agglomeration.

Some general conclusions about reactivity can be drawn from the literature:

- Reactivity generally increases as a function of reaction temperature
- High reactivity has also been seen at rather low temperatures in some cases
- The reduction reactivity is faster with syngas (H_2, CO) than with CH_4 as a fuel
- Nickel oxides and copper oxides are considered to be the most reactive carrier materials developed so far
- Nickel oxides cannot fully convert the fuel gases to CO_2 and H_2O, and reduced Ni catalyzes carbon formation and steam reforming.

Another important characteristic of the metal oxide is its oxygen transport capacity R_o

$$R_O = \frac{M_{ox} - M_{red}}{M_{ox}} \tag{2.12}$$

Where:

M_{ox} : The molar mass of fully oxidized oxygen carrier

M_{red}: The molar mass of fully reduced oxygen carrier

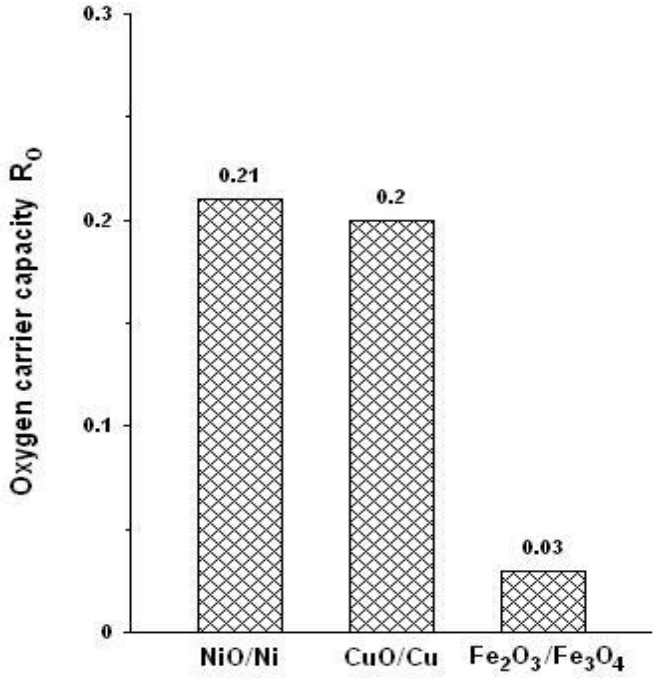

Figure2.6 Oxygen ratios of Ni-, Cu- and Fe-oxides (Adánez et al., 2006).

As seen in Figure 2.6, the higher values of oxygen transport capacities are for NiO and CuO, and it is lower for hematite (Fe_2O_3) in its transformation to magnetite (Fe_3O_4). In spite of the different oxidation states of iron compounds, only the transformation from Fe_2O_3 to Fe_3O_4 may be suitable for CLC systems. The reaction rates for the conversion of hematite to metallic iron are slow, and further reduction to wüstite (FeO) would lead to a high decrease in the purity of CO_2 obtained in the fuel reactor due to the increase of CO and H_2 concentrations in the equilibrium mixture. The transport capacity of the oxygen carriers obviously decreases with the addition of inert filler material (Adánez et al., 2006).

Reactivity experiments, simulating CLC and using natural ores or pure metal oxides as the oxygen carriers, without the presence of inert fillers, have shown rapid degeneration or low reaction rates for these materials. To achieve higher reactivity and get more stable oxygen carriers, these could be prepared synthetically and mixed with an inert material. It is believed that the porosity of the particles is increased with the addition of inert filler and due to that the oxidation and reduction rates of the carrier will be higher. Inert filler also helps to maintain the structure and increases the ionic conductivity of the particles, but on the other hand it decreases the ratio of free oxygen in the carrier (Johansson, 2007). During the last decade extensive research has been conducted on CLC with respect to oxygen carrier development; see Table 2.3 for a review. Transition metal oxides, such as Ni, Fe, Cu, and Mn oxides, were reported as reactive oxygen carrier particles.

Table 2.3 Literature data on oxygen carriers for chemical-looping combustion (Johansson et al. 2006)

Reference	Oxygen carrier (Me_xO_y/support)	Reduction Agent	T_{red} (°C)	D_p (mm)	Apparatus
Nakano et al. 1986	Fe_2O_3, Fe_2O_3-Ni, Fe_2O_3/Al_2O_3	H_2, H_2O/H_2	700-900	0.007	TGA
Jin et al. 1999	NiO/Al_2O_3, NiO/TiO_2, NiO/MgO, CoO/Al_2O_3, CoO/TiO_2, CoO/MgO, Fe_2O_3/Al_2O_3, Fe_2O_3/TiO_2, Fe_2O_3/MgO	H_2, H_2O/CH_4	600, 700	1.8	TGA
Copeland et al. 2000	CuO-based, Fe_2O_3-based on alumina, aluminates and silicates	$CO_2/H_2/CH_4$	800	Fine Powde	TGA
Mattisson et al. 2000	Fe_2O_3, Fe_2O_3/Al_2O_3, Fe_3O_4	CH_4	950	0.12-0.50	FB
Cho et al. 2002	Fe_2O_3/Al_2O_3, Fe_2O_3/MgO	CH_4	950	0.125-0.18, 0.18-0.25	FB
Adánez et al. 2004	CuO, Fe_2O_3, MnO_2, NiO with Al_2O_3, SiO_2, TiO_2, ZrO_2	CH_4/N_2	800, 950	0.1-0.3	TGA, FB
Ishida et al, 2005	Fe_2O_3/Al_2O_3	H_2	900	0.07	TGA
Lyngfelt and Thunman 2005	NiO based, Fe_2O_3 based	Natural gas	560-900	-	CF
Roux et al. 2005	CaO, CuO, Fe_2O_3, MgO, MnO_2, NiO, TiO_2, Al_2O_3	CH_4	550-950	0.0019-0.093	TGA
Abad et al, 2006	Fe_2O_3/Al_2O_3	Natural gas, Syngas, CH_4	800-950	0.09-0.212	FB, CFB
Johansson M. et al. 2006	Fe_2O_3, Mn_3O_4 and NiO on different inerts	CH_4/H_2O	950	0.125-0.18	FB
Scott et al 2006	Fe_2O_3	Lignite + $H_2O/CO_2/N_2$	900	0.300-0.425, 0.425-0.710	FB
Son and Kim 2006	NiO and Fe_2O_3 on TiO_2, Al_2O_3 and bentonite, $NiOFe_2O_3$/bentonite	$CH_4/H_2O/CO_2/N_2$ (TGA) CH_4 (CFzB)	650-950	0.106-0.15	TGA, CFB
Zafar et al. 2006	NiO, CuO, Mn_2O_3, Fe_2O_3 with SiO_2 and $MgAl_2O_4$	$CH_4/H_2O/CO_2/N_2$	800-1000	0.18-0.25	TGA
Johansson M. et al. 2006	Fe_2O_3, Mn_3O_4, CuO and NiO on different inerts	CH_4/H_2O	950	0.125-0.18	FB

TGA = Thermogravimetric analyzer, FB = Fluidized bed, CFB = Circulating fluidized beds, i.e. chemical-looping combustor

2.10 Melting point and mechanical strength

The temperature in which the CLC process operates is invariably between 600 °C and 1200 °C (Hossain & Lasa, 2008). This will limit the oxygen carrier material selection. The melting point of the oxygen carrier should be high enough to withstand the CLC reaction temperature and to avoid agglomeration of circulating particles. Melting points of some suitable metals and inert fillers are listed in Table 2.4. As shown, Cu has a relatively low melting point, and therefore it cannot be used above ~900 °C.

Table 2.4 Physical properties of solids (Adánez et al., 2004).

Active material	Solid density, (kg/m^3)	Melting point (°C)
Cu	8920	1085
CuO	6400	1124 *
Ni	8900	1453
NiO	6670	1955
Fe	6980	1536
FeO	5700	1377
Fe_2O_3	5240	1462*
Fe_3O_4	5180	1597
Inert		
Al_2O_3	3965	2017
SiO_2	2260	1723
TiO_2	4260	1857
ZrO_2	5600	2677
MgO	3580	283

* Normal decomposition point

Adánez et al. (2004) studied the mechanical strength of different oxygen carriers. It was demonstrated that the crushing strength seems to be strongly dependent on the type of active metal oxide and its concentration, the inert filler used as a binder, and the sintering temperature. In general, a higher sintering temperature increases the crushing strength,

but some carriers cannot withstand high temperatures due to decomposition and melting of the involved compounds. Fe-based oxygen carriers, prepared with Al_2O_3, TiO_2 and ZrO_2, and sintered above 1100°C showed high crushing strength values. Cu-based carriers did not show measurable values, except when using either SiO_2 or TiO_2 as inert filler. Conversely, combinations of Ni and TiO_2 or Ni and SiO_2 showed suitable crushing strength values.

2.11 Chemical–Looping Reforming (CLR)

The chemical-looping principle can also be employed for methane reforming and hydrogen production. Chemical-looping reforming (CLR) uses the same basic principles as CLC. The main differences between these two approaches are the target products, in CLR the products are H_2 and CO, instead of heat as in CLC processing.

As shown in Figure 2.7, in the CLR process it is important to select an oxygen carrier that tends to partially oxidize methane to synthesize gas other than CO_2 and H_2O. In addition, the O_2/fuel ratio should be kept low in order to prevent the complete oxidation of the fuel. The oxygen carrier then circulates between the reactors. In the fuel reactor, it is reduced by the fuel to produce CO and H_2, according to Equation (2.13).

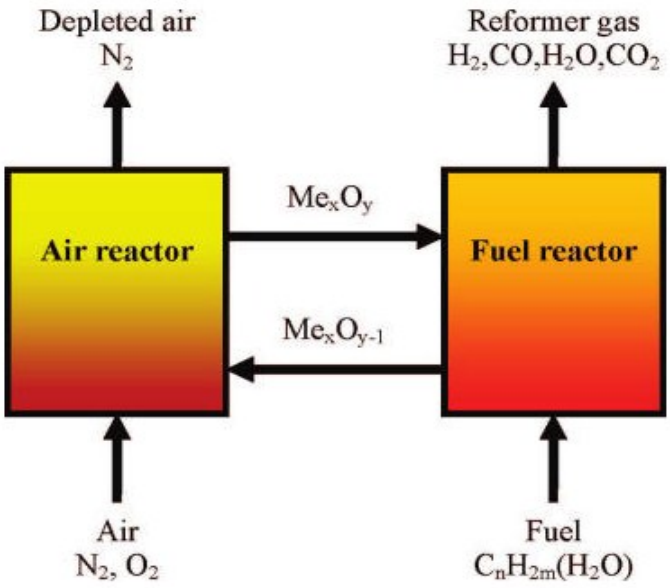

Figure 2.7 Schematic representation of the chemical-looping reforming (CLR) process.

$$Me_xO_y + CH_4 \rightarrow Me_xO_{y-1} + 2H_2 + CO \quad (2.13)$$

Oxygen carrier regeneration:

$$Me_xO_{y-1} + {}^1/_2\, O_2 \rightarrow Me_xO_y \quad (2.14)$$

2.12 Chemical-Looping Hydrogen (CLH) Process

Chemical-looping hydrogen (CLH) generation, which is a variant of the CLC process, is a type of water splitting technique with a redox reaction of a metal oxide. The CLH system is composed of two reactors, an oxidation reactor for water decomposition and a reduction reactor, as shown in Figure 2.8.

A reduction gas is introduced into the reduction reactor, where the metal oxide particles are reduced. The reduced metal oxide is circulated to the oxidation reactor, where it decomposes water to generate H_2. Upon complete conversion of the reduction gas, the exit gas stream from the reduction reactor contains only CO_2 and H_2O, and H_2 is emitted

from the oxidation (or 'water decomposition') reactor. As a consequence, pure H_2 and CO_2 can be obtained with H_2O condensation without a separation process. The hydrocarbon or synthesis gas fuel, used as a reduction gas, is then introduced into the reduction reactor, where it reacts with a metal oxide particle according to the following reactions:

$$(2n + m)Me_xO_y + C_nH_{2m} \rightarrow (2n + m)Me_xO_{y-1} + mH_2O + nCO_2 \quad (2.15)$$

$$Me_xO_y + H_2 \rightarrow Me_xO_{y-1} + H_2O \quad (2.16)$$

$$Me_xO_y + CO \rightarrow Me_xO_{y-1} + CO_2 \quad (2.17)$$

The reduced metal oxide is then circulated to the water decomposition reactor, where it is oxidized with water according to the following reactions:

$$Me_xO_{y-1} + H_2O \rightarrow Me_xO_y + H_2 \quad (2.18)$$

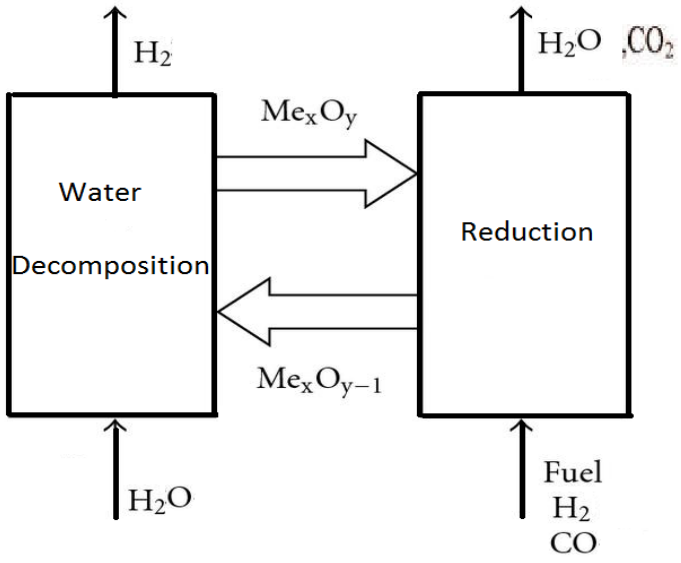

Figure 2.8 Conceptual diagram of chemical-looping hydrogen generation (CLH).

CHAPTER 3 REDUCTION STUDIES

Iron ore reaction with methane can be viewed as a non-catalytic gas-solid reaction. Generally, the reaction rate of such reactions can be controlled by several parameters (e. g. external mass transfer; gas diffusion through the bulk gas to the porous particle surface; penetration and gas diffusion through the product boundary layer to the surface of the unreacted core; chemical reaction between the reductant gas and the oxygen of the lattice at this reaction surface). With this in mind, mass transfer resistance can be reduced by working with high gas flows and small sample masses for experiments conducted using thermogravimetric analysis (TGA) (Zafar et al., 2006).

Some of the previously mentioned steps do not directly contribute to the resistance in some cases; as a consequence we may just consider the step with the highest resistance, i.e. the rate limiting steps controls the iron ore reduction, which is a complex, heterogeneous gas-solid reaction. A heterogeneous process involves a sequence of stages (e.g. reactant must diffuse to the surface of a solid before adsorption occurs, which is then followed by chemical reaction). The rate controlling step cannot be inferred simply from the activation energy value (Coetsee et al., 2002). The reaction rate at which the ore is reduced ultimately determines the economic feasibility of the process technology and, as a consequence, the production rate. Either diffusion or chemical reaction might be the rate controlling step, depending upon temperature. Arrhenius plot of ln k vs. 1/T may no longer be straight but curved, as shown in Figure 3.1 showing regions in which the reaction rate is diffusion controlled and reaction controlled.

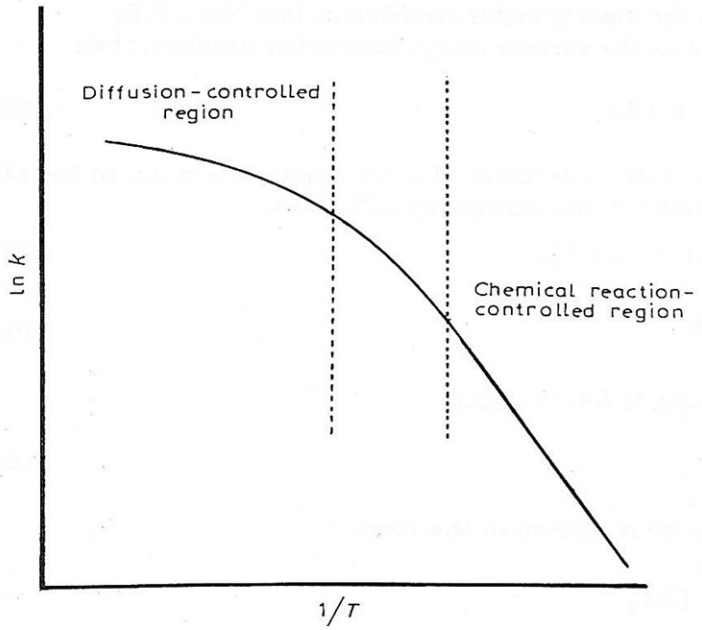

Figure 3.1 The Arrhenius plot for a heterogeneous reaction (Bamford and Tipper, 1980).

3.1 Reduction rate

The iron oxide reduction reaction sequence proceeds in a stepwise manner, following:

$$Fe_2O_{3\ (\text{hematite})} \rightarrow Fe_3O_{4\ (\text{magnetite})} \rightarrow FeO_{(\text{wustite})} \rightarrow Fe \qquad (3.1)$$

According to the obtained experimental results obtained in this study, it appears that at higher temperatures wustite (FeO) and metallic iron (Fe) are the final reduction products. At higher temperatures, also there is potential for coke formation on the particle surface. Summary of activation energy values reported in literature presented in Table 3.1.

Table 3.1 Summary of activation energy values reported in literature (Piotrowski et al 2007).

Source	Reduction step	Reduction mechanism	ΔE_a(kJ/mol)	Experimental method
Shimokawabe (1979)	$Fe_2O_3 \rightarrow Fe_3O_4$	Random nucleation	33.27–74	Linear heating rate
Piotrowski et al. (2007)	$Fe_2O_3 \rightarrow FeO$	Phase boundary	58.13	Isothermal TGA
Sastri et al. (1982)	$Fe_2O_3 \rightarrow Fe$	Phase boundary	57–73	Isothermal TGA
Tiernan et al.(2001)	$Fe_2O_3 \rightarrow Fe_3O_4$	Not determined	106	Linear heating rate
Tiernan et al. (2001)	$Fe_2O_3 \rightarrow Fe_3O_4$	Phase boundary	96	CRTA "rate-jump"
Trushenski et al.(1974)	$Fe_2O_3 \rightarrow Fe_3O_4$	Non-topochemical approach, complex model	69–100	Isothermal TGA
	$Fe_3O_4 \rightarrow FeO$		64.46–78.27	Isothermal TGA
	$FeO \rightarrow Fe$		115.94	Isothermal TGA
El-Geassy et al.(1977) and (1996)	$Fe_2O_3 \rightarrow Fe$	Phase boundary limited by gaseous diffusion	31.6–53.57	Isothermal, 200 μm size
	(Fe_3O_4, FeO, Fe_3C, C present)		9.54–21.51	Isothermal, 100 μm size
Nasr et al. (1996)	$Fe_2O_3 \rightarrow Fe$ (FeO, Fe_3C, Fe_2C, C present)	Initial stage,combination of gaseous diffusion and interfacial chemical reaction	28.92	Isothermal TGA
		Final stage, $T < 900$ °C, gaseous diffusion	23.81	Isothermal TGA
		Final stage, $T > 1000$ °C, gaseous diffusion	14.98	Isothermal TGA
Moon et al. (1998)	$Fe_2O_3 \rightarrow FeO$ (H_2); $Fe_2O_3 \rightarrow FeO$ (CO)	Chemical surface reaction, intraparticle diffusion through the reduced layer	19.84–42.15	Isothermal TGA
Kang Seok Go (2008)	$Fe_2O_3 \rightarrow Fe_3O_4$	Not determined	271	Isothermal TGA

3.2 Experimental

3.2.1 Thermogravimetric Analysis

Thermogravimetric analysis is a technique for thermal analysis; it could be defined as a technique in which a physical property of a substance and/or its reaction products is measured as a function of temperature while the sample is subjected to a controlled temperature program. TGA also measures the rate of change in the weight of a material as a function of either temperature or time in a controlled atmosphere. In order to obtain the best kinetic parameters, the three parameters of weight, temperature, and temperature change should be measured with a high degree of precision. TGA is commonly used to determine:

- Characteristics of materials
- Degradation temperature
- Absorbed moisture content of materials
- Organic and inorganic level in materials
- Decomposition points of explosive and solvent residues (Brown2008)

3.2.2 Experimental apparatus

TGA consists of a high-precision balance into which the sample should be loaded in an alumina crucible, which is placed on a sample holder. It has a platinum thermocouple to measure the temperature. During the entire process an inert purge gas should be introduced to avoid other undesired reactions. A typical thermogravimetric analysis (TGA) commercial system is shown in Figure 3.2.

Figure 3.2 Thermal Gravimetric Analyzer Apparatus (TGA)**.**

3.2.3 Experimental procedure

The reactivity of typical oxygen carriers should normally be investigated initially in a laboratory scale reactor; TGA can be used for this purpose. However, to simulate the process more completely, and gain a better understanding of the process, further experiments should be conducted in a larger system such as a circulating fluidized bed, in which the oxygen carrier can continuously circulate between reactors. In this study analyzing the reactivity of the oxygen carrier were analyzed using an SDT Q-600 TGA system (TA Instruments, New Castle, DE, USA). performed using a TGA instrument (as shown in Figure 3.2).

The oxygen carrier was loaded in an alumina (Al_2O_3) crucible; the sample weight used depends on the density of the oxygen carrier and the gas flow rate. The experiments were carried out isothermally. The experiments Prior to the reduction step, samples of Fe_2O_3 iron ore were preheated (20°C/min) under an inert (argon) atmosphere to the desired temperature (800–950°C). An equilibrium starting temperature of 50°C is used in order to detect possible drying of the sample then heat up to predetermined temperature using dynamic temperature ramp 20°C/min. The final temperature is usually high (e.g. 900°C).

After reaching the desired temperature, the reducing gas (CH_4) was then introduced during an isothermal hold (i.e. fixed temperature) with a flow rate of in range of 15-20 ml/min. The initial weights of the Fe_2O_3 samples were between 20 and 60 mg. The reduction kinetics was determined by monitoring the weight change of the sample during its reduction under isothermal conditions. The TGA analytical apparatus microbalance sensitivity is 0.1 μg. The gas flow into the reactor was controlled using an electronic mass flow regulator. Argon was used as an inert carrier gas for dilution of the methane. For the majority of the experiments the reducing gas composition was 70% CH_4 in argon as a carrier inert gas. A Summary of the reaction conditions used is presented in Table 3.2.

Table 3.2 Summary of experimental conditions and methods

Particle	Iron ore (Fe_2O_3 200 micron)
Temperature (°C)	Isothermal hold (850, 875, 910, 930, 945, 950°C)
Purge gas	Ar (40, 100 ml/min)
Reactant gas (Reduction)	CH_4
Method	Initial: 50°C Ramp: 20°C/min to target temprature Isothermal: (20, 60, 80 min)

X-ray diffraction (XRD) analysis was carried out by powder XRD patterns acquired using a high speed X-ray diffractometer (Model: Bruker D8 Advance), using Cu-Ka radiation having a wave length of 1.54 A˚ , tube voltage of 40 kV, and tube current of 40 mA. Selected samples were characterized prior to and following the reactivity testing, using powder XRD. Also morphological characterization of the selected samples was performed by using the HITACHI S-4700. Samples were papered a day prior to the SEM test, silver paste was used in sample preparation. Measurements were performed at accelerating voltage=15KVolt, emission current=22500 nA, and working distance=12200 um.

3.3 Iron oxide

It is important that the metal oxide has a sufficient reduction and oxidation rate. It is also an advantage if the metal oxide is inexpensive and environmentally benign. A number of different metals mentioned earlier are possible candidates: Cu, Ni, Cd, Zn, Fe and Co. A detailed review of potential oxygen carrier candidate in the literatures implies that Cu-based oxygen carrier has quite good reactivity, exothermic reduction reaction, but low melting point and tendency to agglomeration due to intensive heat. Ni-based oxygen carriers are most reactive, thermally stable, but toxic and most expensive. Cd and Zn are not suitable at all because of low melting point. Fe-based oxygen carriers are cheap, readily available, endure physical stress and heat but less reactive.

In the present study the iron oxide ore, natural hematite, was picked as an oxygen carrier, based on the advantages mentioned earlier in (Section 2.4). The iron ore used was obtained from the Iron Ore Company of Canada, IOC, in the form of small pellets with an average diameter of 1.5 centimeter. Various binders, such as Al_2O_3, SiO_2, CaO, etc. were added to the iron ore to make the pellets. An ICP-OES metal scan of the iron ore used as oxygen carrier is presented in Table 3.3. These additives increase the mechanical strength, reactivity and ionic conductivity of the iron ore as an oxygen carrier agent. The ore was ground to different particle sizes (e.g. 50 to 200 micron) with a ball mill; then it was sieved to have a uniform powder size through different size meshes. It would be best for the process if the particle size distribution were narrow. It can be presumed that the impurity additives act as inert components.

Table 3.3 ICP metals scan of the iron ore.

Oxide	Al_2O_3	BaO	CaO	Cr_2O_3	Fe_2O_3	K_2O	MgO	MnO	Na_2O	SiO_2	SrO	TiO_2	V_2O_5	ZrO_2
Wt. %	0.27	<0.01	0.65	0.02	97.71	0.02	0.31	0.09	0.03	0.78	<0.01	0.07	0.01	<0.01

3.4 TGA Data Evaluation

TGA experiments were conducted for the reactivity analysis of the oxygen carrier under specific, pre-determined conditions. Weight variation, as a function of time was monitored during the reduction experiments. The experiments were carried out isothermally. Figure 3.3 shows a typical weight variation of the CLC process, as it can be seen during reduction cycle mass losses and later, oxidation cycle, a mass gain trend is observed. But in this study the objective is to study reduction reaction then the mass loss is the phenomena observed in the experiments.

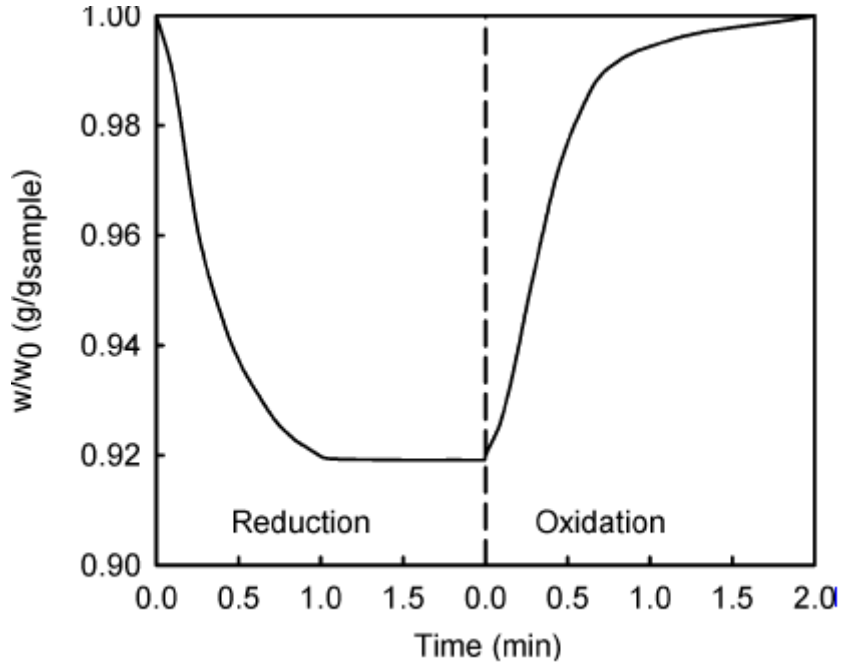

Figure 3.3 Typical weight variation of an oxygen carrier in a TGA test of the CLC process (Adanez et al. 2004).

In practice, Fe_2O_3 is reduced to other forms of iron oxide, such as wustite (FeO) and magnetite (Fe_3O_4). The stages of the iron oxide reduction with methane and consecutive oxidation are as follows:

- $CH_{4\,(g)} + 12\,Fe_2O_{3\,(s)} \rightarrow CO_{2(g)} + 2H_2O_{(g)} + 8\,Fe_3O_{4(s)}$ (3.2)

- $CH_{4\,(g)} + 4\,Fe_2O_{3\,(s)} \rightarrow CO_{2(g)} + 2H_2O_{(g)} + 8\,FeO_{(s)}$ (3.3)
- $CH_{4(g)} + {}^{4}/_{3}\,Fe_2O_{3\,(s)} \rightarrow CO_{2(g)} + 2H_2O_{(g)} + {}^{8}/_{3}\,Fe_{(s)}$ (3.4)

According to the above reactions' stoichiometry, the first reaction corresponds to a 3.34% mass loss and the other ones result in 10% and 30% decrease, respectively, in the initial mass of the sample (see Table 4.1). The degree of conversion, α, as a function of time (t), was obtained from Equation (3.5) detail will be discussed in the next chapter.

$$\alpha(t) = \frac{m_0 - m(t)}{m_0 - m_x} \quad (3.5)$$

The degree of conversion, as a function of time (t), calculated using Equation 3.5; an experimental set is presented in Figure 3.4.

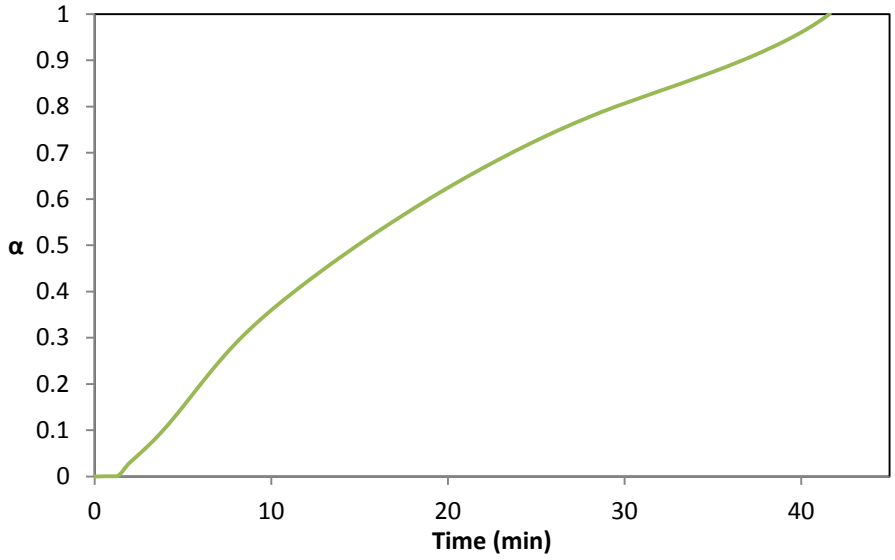

Figure 3.4 Conversion –time plot for a 80 min isothermal experiment based on $Fe_2O_3 \rightarrow Fe_3O_4$.

3.5 Kinetic Model

The kinetics of the reduction reaction(s) have been thoroughly investigated in the present study. Several rate limiting stages can affect the reaction rate (e.g. internal mass transfer and external mass transfer). Working with small sample masses in the TGA experiments, together with high gas flow rates, would reduce mass transfer resistance (Zafar et al., 2006). To determine whether the internal mass transfer and/or external mass transfer were affecting the reaction rate, the sample weight and the gas flow rate were varied in the ranges 20 to 60 mg and 15 to 40 mL/min respectively.

To obtain the kinetic model a mathematical equation should be employed. Weight data could be converted to conversion degree employing Equation 3.5. The obtained conversion data were analyzed using the mathematical models presented in Table 3.4. This approach will be discussed in detail in Chapter 4. The temperature dependence of the kinetic constant was assumed to be Arrhenius type (Equation 3.6); the activation energy could be determined from the slope of the plots of Equation 3.7.

$$k = k_0 e^{-E/RT} \tag{3.6}$$

$$\ln k = \ln k_0 - \frac{E}{RT} \tag{3.7}$$

There are several mathematical models developed for gas-solid reactions, which are presented in Table 3.1. The most commonly used solid-state reaction equations are presented in Table 3.4. The functions D_1 through D_4 represent diffusion equations. R_2 and R_3 are the equations for the phase-boundary-controlled reactions, for cylinder and sphere geometries, respectively. F_1 is the function for first-order reactions. A_2 and A_3 are for the Avrami-Erofe'ev equations. This method compares the experimental data, in the form of fraction reacted, α, versus time. Validity of the functions should be investigated to determine the reaction mechanism; it varies depending on the experimental condition used which presented in Table 3.4.

Table 3.4 Solid-State Reaction Rate Equations (Hancock and Sharp1972).

Function	Equation	Model	Equation number
D_1	$\alpha^2 = kt$	Diffusion	3.8
D_2	$(1-\alpha)\ln(1-\alpha)+\alpha = kt$	Diffusion	3.9
D_3	$[1-(1-\alpha)^{1/3}]^2 = kt$	Diffusion	3.10
D_4	$1-2\alpha/3-(1-\alpha)^{2/3} = kt$	Diffusion	3.11
F_1	$-\ln(1-\alpha) = kt$	First order reaction	3.12
R_2	$1-(1-\alpha)^{1/2} = kt$	Phase-boundary-controlled	3.13
R_3	$1-(1-\alpha)^{1/3} = kt$	Phase-boundary-controlled	3.14
Zero order	$\alpha = kt$		3.15
A_2	$[-\ln(1-\alpha))]^{1/2} = kt$	Avrami-Erofe'ev	3.16
A_3	$[-\ln(1-\alpha)]^{\frac{1}{3}} = kt$	Avrami-Erofe'ev	3.17

CHAPTER 4 RESULTS AND DISCUSSION

The following chapter outlines the experiments performed to determine the likely mechanism(s) of reduction of Fe_2O_3 in a methane-containing environment. The first segment of the chapter describes the experimental data obtained. The experiments were performed using an isothermal approach, in order to determine the reaction kinetics curves, with the TA Instruments SDT Q600. This instrument has a differential thermal analysis sensitivity of ±0.001ºC, using a Pt/Pt-Rh thermocouple (Type R). A typical example of a TGA curve of the weight change during a reduction reaction experiment is shown in Figure 4.1. The conversion degree of iron oxide is then computed using Equation (3.5), and the reduction conversion of iron ore at different temperatures is shown in Figure 4.2. In the second part of this chapter, the focus is on assessment of the reduction kinetics and the underlying reaction mechanism that may be occurring, together with an examination of the morphology of reaction products.

4.1 Kinetic analysis

As noted above, an example of a typical TGA curve obtained for the iron ore is shown in Figure 4.1. To analyze the reactivity of iron oxide, isothermal plots of the conversion factor α (t), based on both Fe_3O_4 and FeO formation, and calculated using Equation 3.5, are then developed from the TGA curves. Examples of the conversion curves that are obtained for five different temperatures are shown in Figure 4.2. All of the isotherm curves have a generally sigmoidal shape, which shows three distinct regions. The first of these regions highlights the induction period ($0 < \alpha < 0.15$), which is usually regarded as the development of stable nuclei. Then, an acceleratory period of growth phenomena for the nuclei is observed ($0.15 < \alpha < 0.5$). The final region in the curves is the deceleration or decay period ($0.5 < \alpha < 1$), which corresponds to the termination of growth due to the impingement and consumption of reactant, and leads to the deceleration period (Bamford and Tipper, 1980).

Depending upon the length of the reduction segment, the final state of the iron oxide would differ; the main reactions that can happen are presented in Table 4.1, together with the associated theoretical weight changes that arise. Typical weight variations seen in a 70 min test are presented in Figure 4.1. In addition, it can be observed there are two major inflection points along the plot, which show FeO and Fe formation and correspond to ~10% and ~ 30% reduction, respectively. There is a slight difference between the experimentally observed values and the theoretical one, which presumably accounts for added impurities. As noted above, the calculated conversion-time plots are presented in Figures 4.2. It can be inferred from these plots that the reaction rate increases with temperature. The reaction rate also increases with increasing methane content in the inlet gas (i.e. as a ratio with the Ar carrier gas) (see Appendix D for examples).

Table 4.1 Possible reduction reactions and the associated theoretical weight loss that can occur for Fe_2O_3 reduction.

X	**Reaction**	**Equation No.**
3.34 %	$Fe_2O_3 \rightarrow Fe_3O_4$	4.1
10%	$Fe_2O_3 \rightarrow FeO$	4.2
30%	$Fe_2O_3 \rightarrow Fe$	4.3

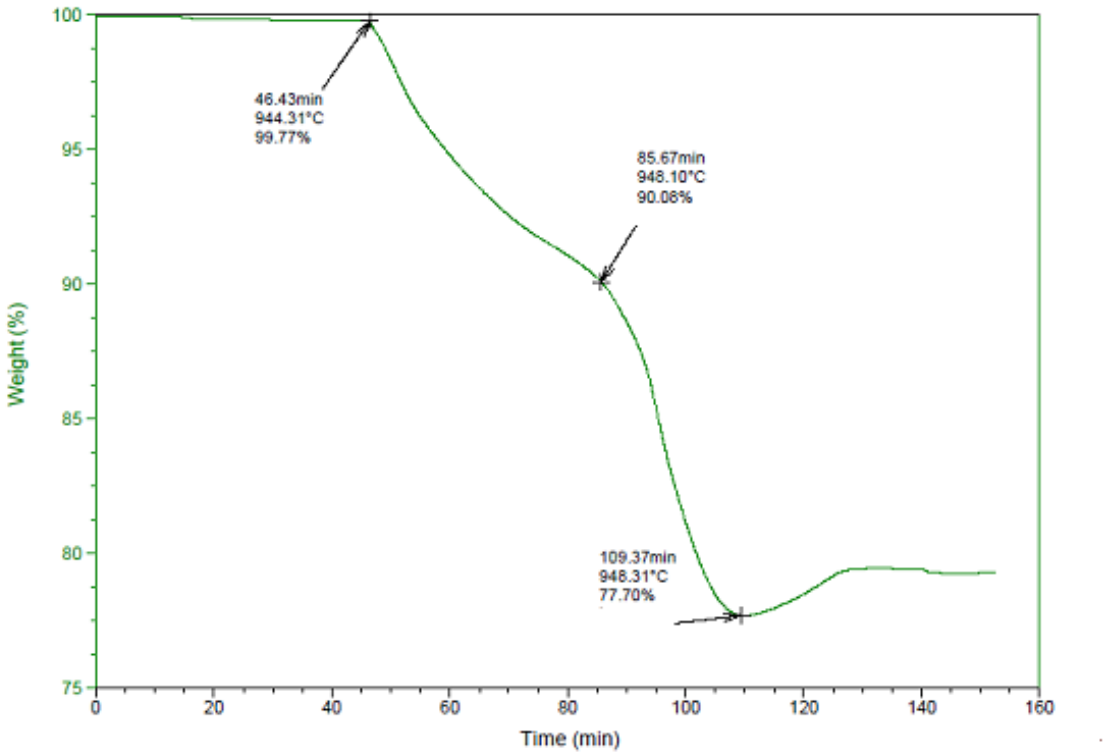

Figure 4.1 An example of the TGA results obtained for a 70 min reduction experiment using iron ore at 950 ºC 40 Ar: 20 CH_4.

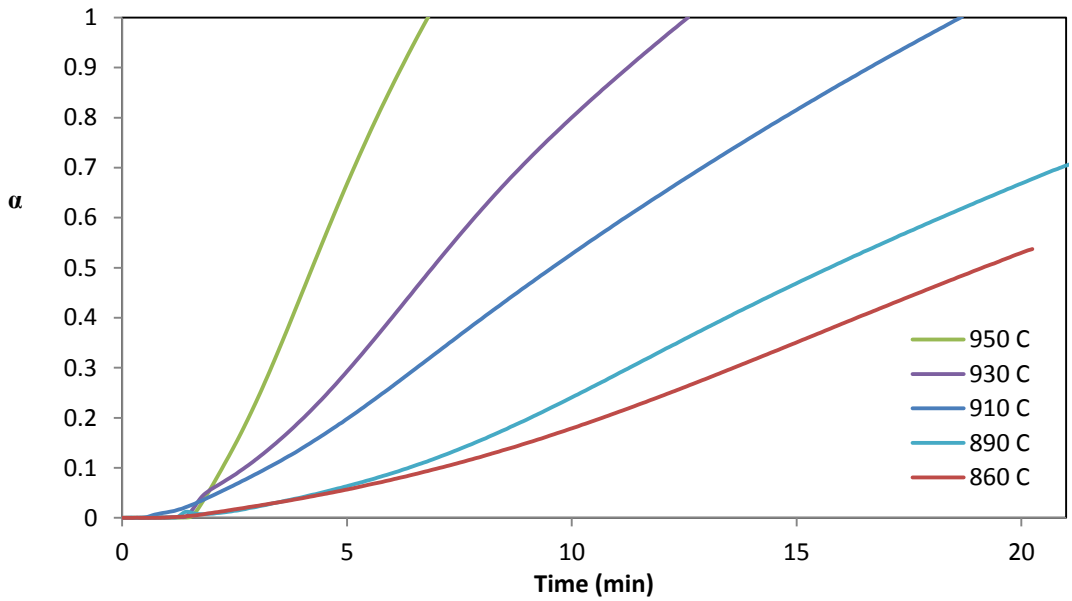

Figure 4.2 Conversion factor (α) vs. time for 80 min isothermal experiments are various temperatures (based on conversion of $Fe_2O_3 \rightarrow Fe_3O_4$).

4.1.1 Kinetic parameters

To obtain the kinetic model, ideally an appropriate mathematical equation should be employed to convert the obtained TGA sample weight data. For the present work the obtained weight variation data were converted to the conversion factor (α) by using Equation (3.5). Then, by employing the solid state functions presented in Table 4.2, the obtained conversion factors were correlated with those functions to find the best fit. The reaction rate constant (k) then computed from the slope of the best fitted model.

Table 4.2. Solid state reaction rate equations assessed in the present work (Piotrowski2005).

Reaction Equation	Reaction Mechanism	Equation No.
$1-(1-\alpha)^{1/3}=kt$	Phase boundary control reaction	4.4
$-\ln(1-\alpha)=\mathrm{kt}$	First order reaction	4.5
$[-\ln(1-\alpha))]^{1/2}=\mathrm{kt}$	Avrami-Erofe'ev (Phase change model)	4.6
$\left[1-\sqrt[3]{\frac{100-\alpha}{100}}\right]^2=kt$	Jander (Diffusion controlled)	4.7
$\left[1-(1-\alpha)^{1/3}\right]^2=kt$	Jander (Diffusion controlled)	4.8
$1-\frac{2}{3}\alpha\ (1-\alpha)^{2/3}=kt$	Ginstling-Brounshtein (Diffusion controlled)	4.9

As discussed earlier, based on the controlling step in the course of the reaction such as diffusion models, phase boundary models, or chemical reaction models, the experimental data could be fitted to one (or more) of the equations that represent controlling mechanism. Some of the correlated functions are presented in Figures 4.4 to 4.8, and the model exhibiting the best fit can then represent the likely experimental reaction mechanism.

Based on assessment of this curve fitting, initially the reduction reaction is phase boundary controlled and the kinetic parameters were evaluated using Equation 4.6. Once a thin layer of iron oxide (i.e. Fe_3O_4) is formed; the diffusion control is clearly the

controlling mechanism of reaction course. Hence, the diffusion models (i.e. the Jander and Ginstling-Brounshtein) presented in Table 4.2 can successfully represent the experimental data. The diffusion equation validity is confirmed after a specific period of time, shown in Figures 4.6 and 4.7, by applying the presented equations to the experimental data the reaction rate constant can be estimated.

In the initial stage of the reaction ($Fe_2O_3 \rightarrow Fe_3O_4$) the lattice transforms from rhombohedral to cubic so the reduction behaviour is different, as it incorporates a crystalline phase change. In the later transformation ($Fe_3O_4 \rightarrow FeO$), both phases have a cubic crystalline structure, and nominally no phase change occurs. The phase–boundary-controlled reaction is linear during the early stages of the reaction, and this consequently confirms the surface controlled reaction at the beginning of the process. Upon regression analysis on the obtained data, it can be concluded that overall the Avrami-Erofe'ev phase change model is best suited to model the experimental results.

The activation energy of the process and the pre-exponential factor were determined from the Arrhenius plots, using kinetic constant (k) (concerning intrinsic Avrami-Erofe'ev kinetics) were then applied to obtain activation energy value from the Arrhenius equation. The ln(k) plot is a straight line with a negative slope (see Figure 4.8) the experimental data at various temperatures presented in Table 4.3 . The resulting activation energy was determined to be 215 kJ/mol and the intercept of the Arrhenius plot represents pre-exponential factor k_0 which in this case study is 287002074 min^{-1}.

The activation energy of the process and the pre-exponential factor were determined from an Arrhenius plot, using the kinetic constants (k) determined at various temperatures (Table 4.3). The resulting activation energy was determined to be 215 kJ/mol (Figure 4.3). It could be implied that early stage of reaction demands higher activation energy in comparison to the later stage.

It could be implied that early stage of reaction demands higher activation energy in compare to later stages of the reduction. Also the obtained activation energy is rather

high in comparison to the previously reported data in Table 3.1. It could be concluded that the addition of the previously mentioned elements, reported in the ICP-OES metal scan (Table 3.3), affects the activation energy of the reduction reaction.

Table 4.3. Data determined for the activation energy calculation (shown in Figure 4.3).

T (ºC)	1/T	*k*(kJ/mol)	Ln *k*
875	0.000871	0.0444	-3.11452
910	0.000845	0.0805	-2.5195
930	0.000831	0.1233	-2.09313
945	0.000821	0.1592	-1.83759
950	0.000818	0.1763	-1.73557

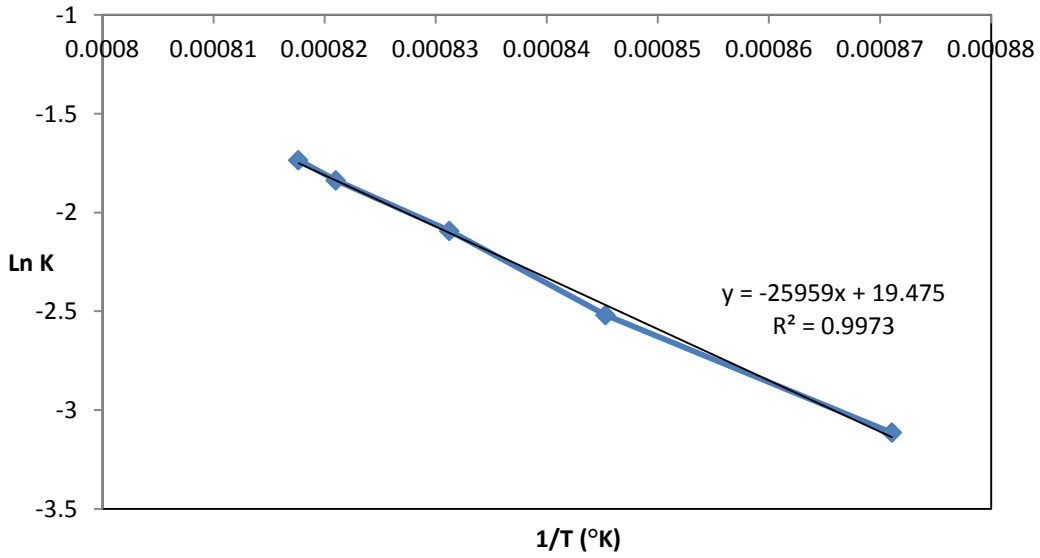

Figure 4.3 An Arrhenius plot of ln k vs. 1/T, which is used for determination of the activation energy.

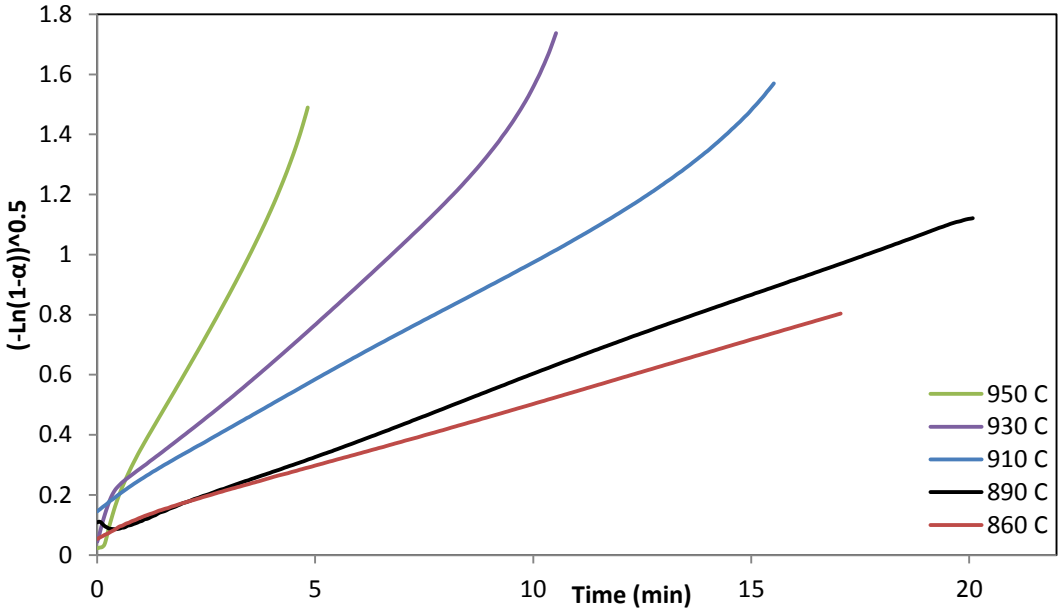

Figure 4.4 Avrami-Erofe'ev equation (Phase change model) vs. time for 20 min isothermal experiment (based on Fe_3O_4).

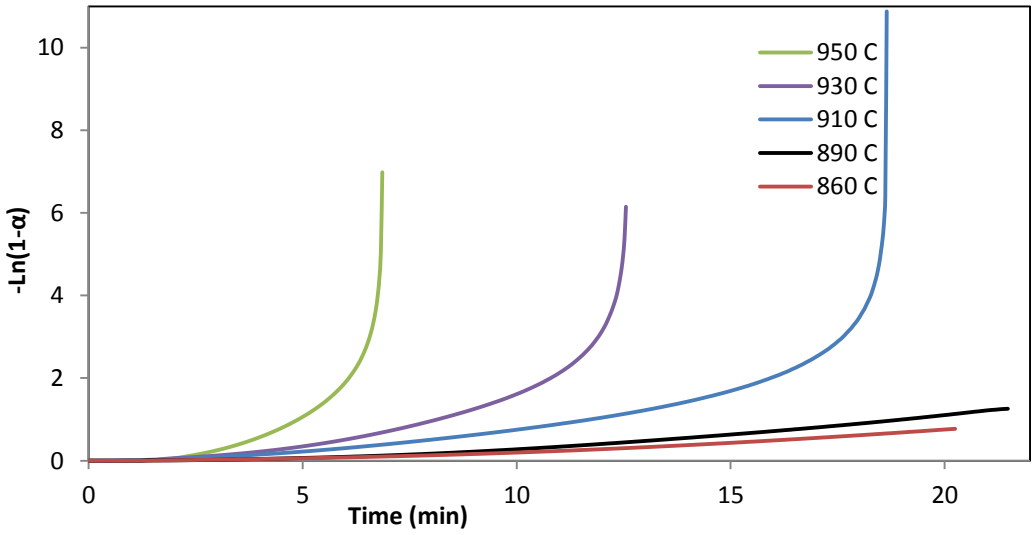

Figure 4.5 A plot of –Ln(1-α) vs. time for the conversion data (first order reaction).

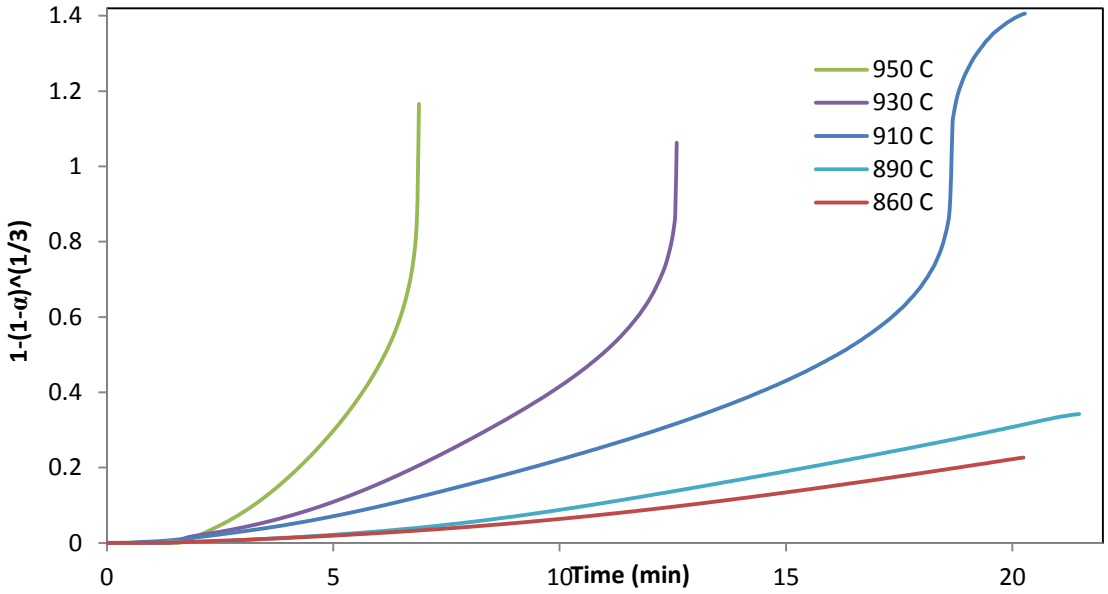

Figure 4.6 A plot of 1-(1-α)^(1/3) vs. time for the conversion data *(*phase boundary control reaction model).

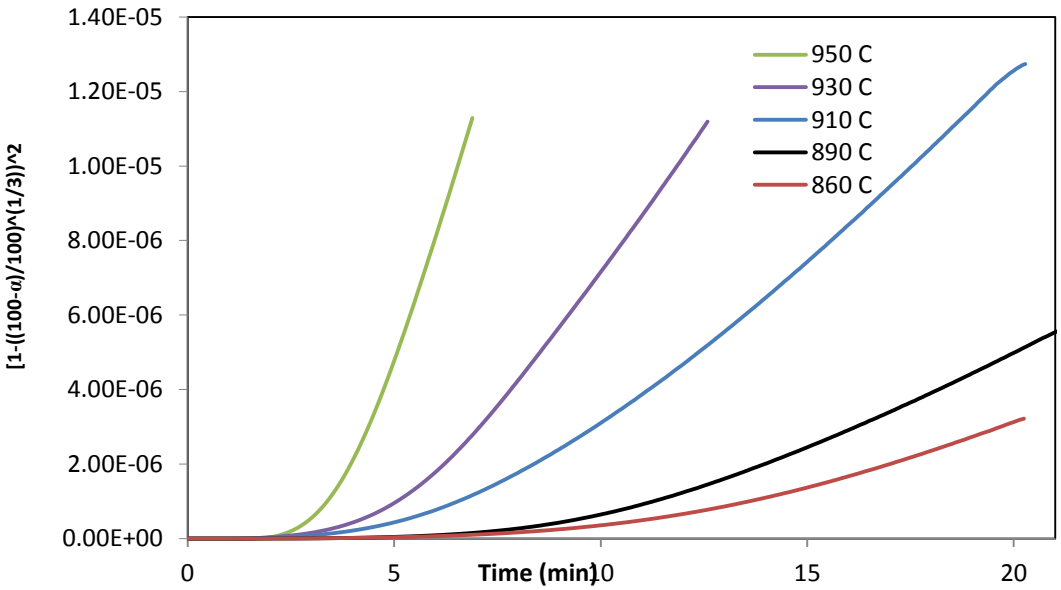

Figure 4.7 A plot of the Jander equation (Equation 4.7) for the diffusion controlled model.

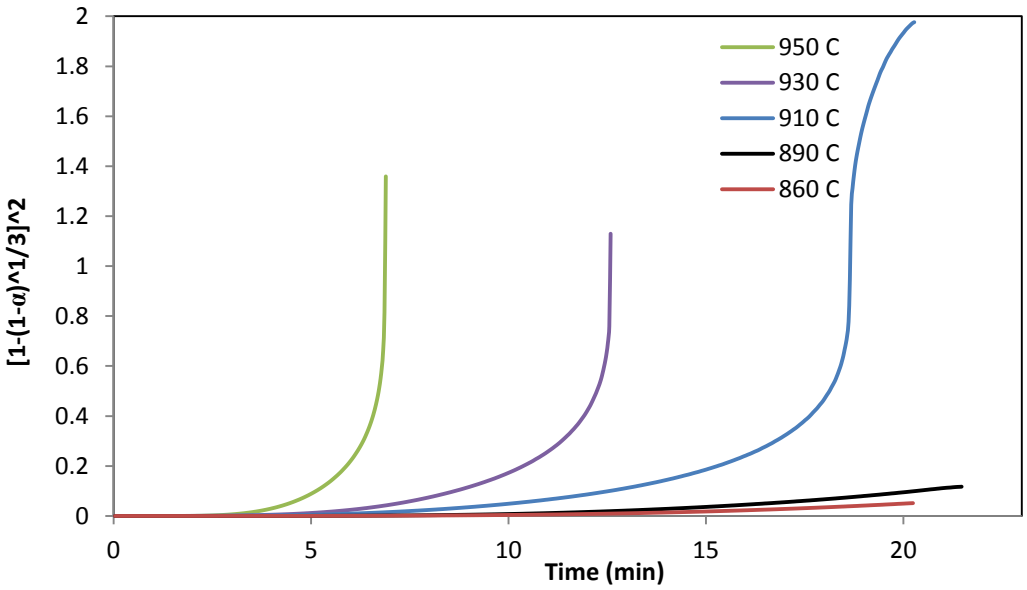

Figure 4.8 A plot of the Jander equation (Equation 4.8) for the diffusion controlled model.

From the obtained results it was observed that, the reaction rate was not affected by the sample mass. However, it was observed that increasing the reductant gas (CH_4) concentration, by altering the Ar: CH_4 ratio will increase the reduction rate. For the present case the following Ar: CH_4 volume ratios were examined: $30Ar:20CH_4$, $40Ar:20CH_4$, $100Ar:20CH_4$, $100Ar:15CH_4$, and $90Ar:15CH_4$. The data obtained for these tests is summarised in Appendix D.

4.2 X-ray Diffraction and scanning electron microscopy

The X-ray diffraction (XRD) method was used for identification of the crystalline chemical species, while the scanning electron microscope (SEM) was applied to characterize the surface morphology, as well as the chemical properties of both the initial and reduced iron oxide particles using energy dispersive X-ray spectroscopy (EDS). This characterization was performed in order to aid in gaining an understanding of the chemical and physical transformations happening during the reduction reaction.

In particular, SEM can highlight changes in the surface morphology of the powders, notably changes in the roughness, while EDS can determine chemical changes. In

particular, this is useful for assessing potential carbon deposition during the reduction process (i.e. from the methane gas ,it revealed that gasification of samples at high temperature causes the pore sizes had been enlarged by the thermal stress during reaction. Particle fracture could occur through thermal stress (phase changes leading to cracking). More likely cracking happened due to expansion/contraction when converting through the oxide sequence. The SEM images presented in Figure 4.9-4.12.

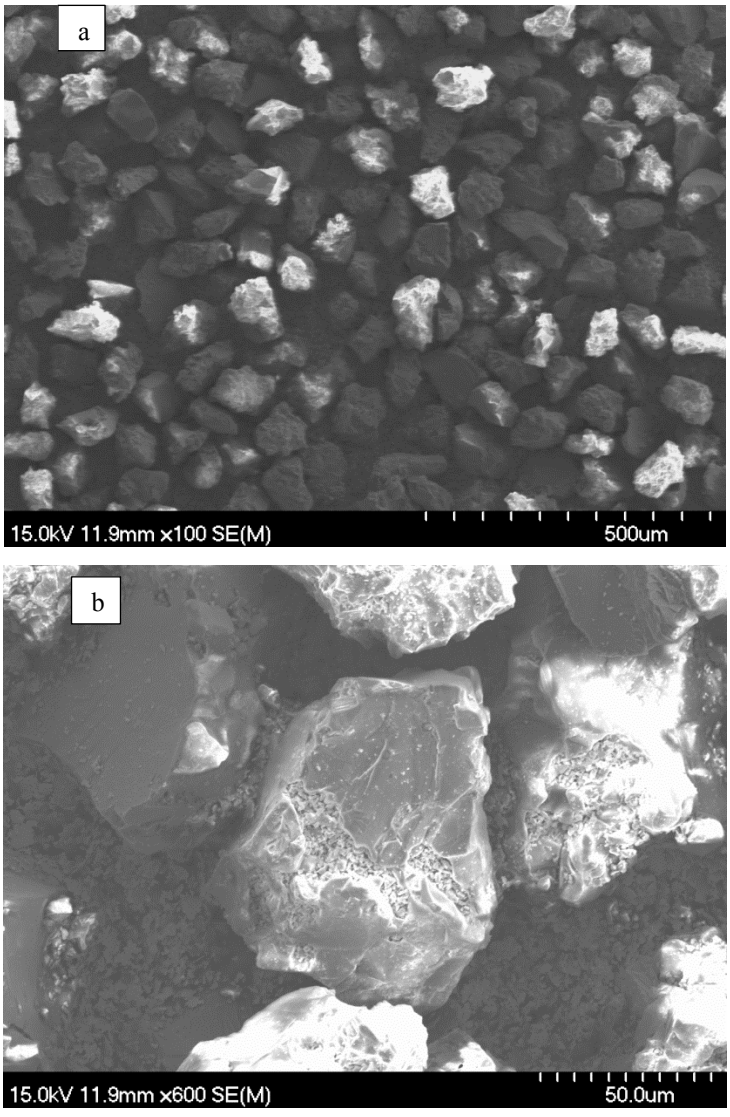

Figure 4.9 SEM images of the as-received iron ore: (a) 100x and (b) 600x magnification.

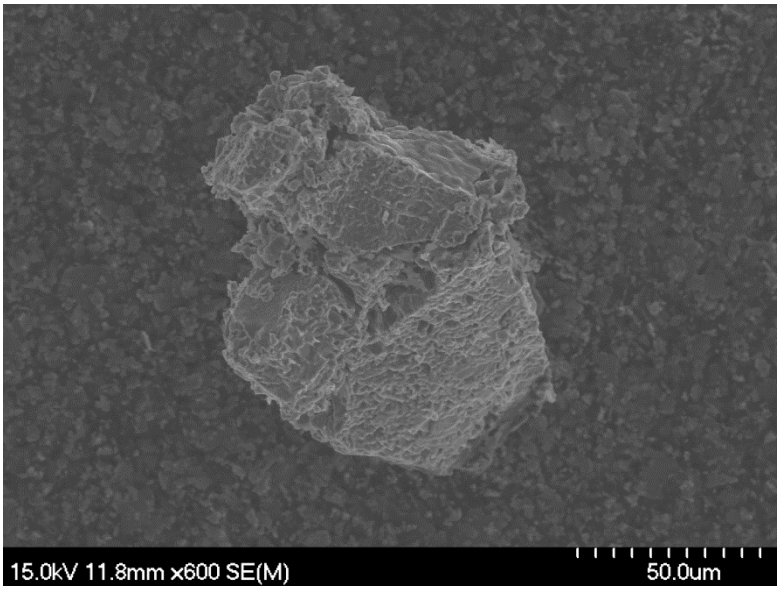

Figure 4.10 An SEM image of sample A (Conditions: T=950 ^{o}C,100ml Ar/15 ml CH_4, 80 min isothermal hold) 600x magnification.

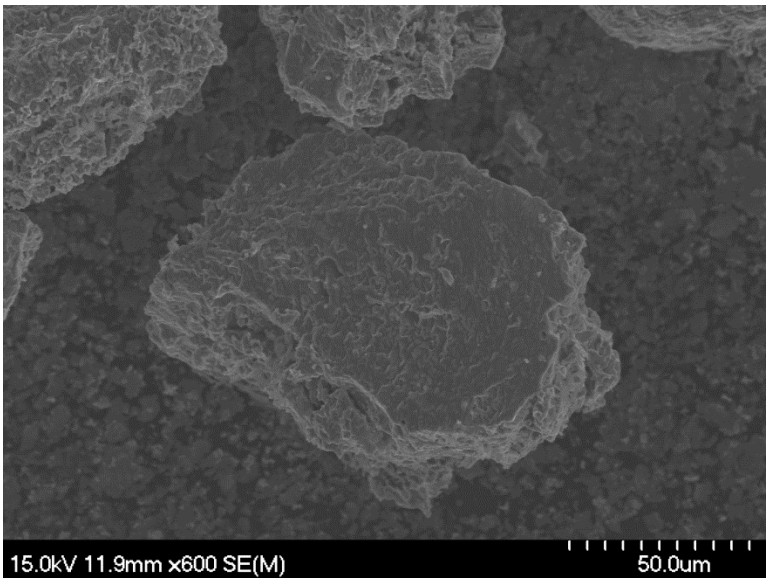

Figure 4.11 An SEM image of sample B, (Conditions: T=950 ^{0}C, 90ml Ar/15ml CH_4, 80 min isothermal hold) 600x magnification.

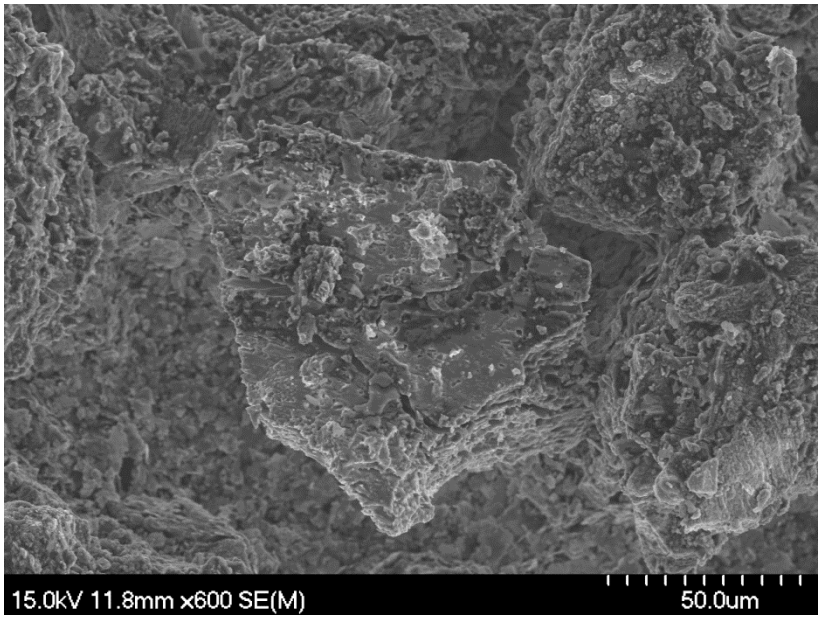

Figure 4.12 An SEM image of sample E (Conditions: T=950 ^{0}C, 40ml Ar/20ml CH_4, 15 min isothermal hold) 600x magnification.

There are two potential mechanisms of carbon deposition: methane decomposition (pyrolysis) and the Boudouard reaction. Pyrolysis is an endothermic reaction more likely occur at high temperatures, typically 750 to 950 °C. The Boudouard reaction is exothermic, and therefore likely to occur at lower temperature. In this study the experiments were conducted at high temperature so pyrolysis is believed to be responsible for carbon formation. The EDS analysis of the samples confirmed carbon deposition on the iron ore particles after reduction at the highest temperatures (this information is presented in Appendix A).

The SEM images shown in Figure 4.9 to 4.12 have been employed for morphology studies of the iron ore samples. It is revealed that gasification of samples at high temperature causes a significant change in the surface morphology, which becomes far more rough than the as-received particles. There is also extensive cracking observed in the particles, which can be attributed to the stresses developed during the reduction reaction (i.e. through phase-change and lattice parameter change). Particle fracture could therefore occur through this mechanical stress (i.e. phase changes leading to cracking/fracture). It is also possible that some thermal stress is generated during heating/cooling, which may contribute to this effect.

CHAPTER 5 CONCLUSIONS AND RECOMENDATIONS FOR FUTURE WORK

The aim of this work was to determine the reaction kinetics of the fuel reactor in the chemical-looping combustion (CLC) process, and to determine the performance of iron ore as an oxygen carrier by evaluating the parameters that increase the reaction rate. An isothermal approach was used to investigate the kinetics of the reduction reaction. Experiments were carried out using a thermogravimetric analyzer (TGA) to assess weight change during the reaction process.

Iron ore was used as an oxygen carrier due to its reduction-oxidation (redox) properties, and the fact that it is environmentally safe and of low cost. In general, the oxygen carrier used in the CLC process is combined with an inert filler material, which acts as a porous support providing a variety of performance benefits (e.g. a higher surface area, increased mechanical strength and attrition resistance, etc.). The raw materials, supplied by the Iron Ore Company of Canada, have some of those metal oxides added to the iron ore pellets, as shown in Table 3.3, to make it a suitable candidate as an oxygen carrier for the CLC process. The structure was also assessed using scanning electron microscopy (SEM) and X-ray diffraction (XRD). It is evident that a higher surface area would increase the reaction rate.

Methane (CH_4) was used as a reducing agent in the present work, diluted with an argon carrier gas. Iron oxide reduction proceeded in a stepwise manner following the sequence $Fe_2O_3 \rightarrow Fe_3O_4 \rightarrow FeO \rightarrow Fe$. Since the reduction of iron ore reaction is complex, as several reactions occur together, it is necessary to understand the kinetics of reduction of the iron ore.

To see the impact of temperature on the reaction, a series of rate experiments were performed at different temperatures. When the tests took longer than 20 minutes, at the higher temperatures, it was observed that the particles would become agglomerated.

The influence of the methane concentration was explored by varying the gas flow rate from 15-20 mL/min, in combination with varying the carrier gas flow rate; several CH_4:Ar gas mixture were tested using this approach. However, there is a limitation on the extent of flow rate variation that can be achieved with the experimental apparatus, although it was seen that by increasing the CH_4 concentration even a small amount, the reaction rate would be increased more than expected; these observations are presented in Appendix D.

The effect of temperature on the reactivity was determined with respect to the reaction rate and its mechanism. Specific efforts were made to detect the effect of temperature change on the reaction rate. It was seen that a higher temperature enhances the reaction rate, as shown in Figures 4.1 and 4.3. From these data it could be inferred that the time required for complete conversion at 950 ºC is less than 10 min when using gas feed stream that has 33.3% of methane. However, it should also be noted that the specimens are sensitive to high temperature (i.e. above 960 ºC), as it was seen that in that temperature range iron carbide (Fe_3C) is more likely to form during methane reduction.

It was concluded that temperature is one of the parameters with the most influence on the reaction rate. Based on these results it could be predicted that carbon capture efficiency would be higher at the higher temperatures, taking into account the issues that are presented if the temperature is too high (i.e. particle aggregation, Fe_3C formation, etc.).

The identification of crystalline chemical species was carried out by X-ray diffraction, both before and after the reduction treatments. Post reduction XRD indicated Fe_3O_4 as the major component of the samples, although other states of the reduced iron ore were also noted. In addition, evidence of carbon deposition was confirmed through both the XRD and EDS analysis. The structural changes and the appearance of the cracks were also observed in the ore particles, due to volume changes associated with the redox reaction sequence.

The reduction kinetics of a commercially obtained iron ore were analyzed using TGA experiments through the course of the present research. There are several avenues that could be examined in the future to gain a better understanding of the CLC process reactions. Outlined below are some of the potential aspects that could be explored in future work, which are beyond the scope of this project due to lack of time and appropriate equipment.

1- Oxidation and reduction in successive cycles to determine the redox properties and the stability of the oxygen carrier.
2- Study the effect of particle size on the reduction reaction(s) and rate(s).
3- Use steam with the methane, in order to minimize carbon deposition during the reduction reaction (i.e. following Adanez et al., 2004). This is potentially important as carbon deposition may limit the CO_2 capture efficiency.
4- Use inert binders of known composition, for example Al_2O_3, TiO_2, to potentially improve the reactivity of the oxygen carrier.
5- Pursue prototype testing in a fixed bed reactor.
6- Employ gas chromatography mass spectrometry to analyze the exit gas stream.

BIBLIOGRAPHY

Abad, A., Adanez, J., Garcia-Labiano, F., de Diego, L. F., Gayan, P., & Celaya, J. (2007). Mapping of the range of operational conditions for cu-, fe-, and ni-based oxygen carriers in chemical-looping combustion. *Chemical Engineering Science, 62*(1-2) doi:10.1016/j.ces.2006.09.019

Abad, A., et al. (2006) The use of iron oxide as oxygen carrier in a Chemical-Looping Reactor.Fuel

Adanez, J., de Diego, L. F., Garcia-Labiano, F., Gayan, P., Abad, A., & Palacios, J. M. (2004). Selection of oxygen carriers for chemical-looping combustion. *Energy & Fuels, 18*(2) doi:10.1021/ef0301452

Adánez, J., et al. (2004,5-9 September) Characterization of Oxygen Carriers for Chemical-Looping Combustion. *7th International Conference on Greenhouse Gas Control Technologies*, Vancouver, Canada

Bamford, C. H., Tipper, C. F. H., & Compton, R. G. (1980). *Kinetics and chemical technology*. Amsterdam: Elsevier

Brown, M. E., & Gallagher, P. K. (2008). *Handbook of thermal analysis and calorimetry: Volume 5*. Amsterdam: Elsevier Science.

Cho, P., T. Mattisson, and A. Lyngfelt. (2002).Reactivity of Iron Oxide with Methane in a Laboratory Fluidized Bed - Application of Chemical-Looping Combustion. *Proceedings of the 7th International Conference on Circulating Fluidized beds*, Niagra Falls, Ontario,Canada,: p. 599-606

Coetsee, T., Pistorius, P. C., & de Villiers, E. E. (2002). Rate-determining steps for reduction in magnetite-coal pellets. *Minerals Engineering, 15*(11), PII S0892-6875(02)00120-6. doi:10.1016/S0892-6875(02)00120-6

Copeland, R.J., et al. (2000, March 26-30). A Novel CO_2 Separation System. *The 8th International Symposuim on Transport Phenomena and Dynamics of Rotating Machinery*, Honolulu, Hawaii

ElGeassy, A. A., Nasr, M. I., & Hessien, M. M. (1996). Effect of reducing gas on the volume change during reduction of iron oxide compacts. *ISIJ International, 36*(6) doi:10.2355/isijinternational.36.640

ElGeassy, A. A., Nasr, M. I., & Hessien, M. M. (1996). Effect of reducing gas on the volume change during reduction of iron oxide compacts. *ISIJ International, 36*(6) doi:10.2355/isijinternational.36.640

Elgeassy, A. A., Shehata, K. A., & Ezz, S. Y. (1977). Steel research - effect of silica on reducibility of iron-oxide. *Iron and Steel International, 50*(5)

Gallagher, P. K., Brown, M. E., & Kemp, R. B. (1998). *Handbook of thermal analysis and calorimetry*. Amsterdam [Netherlands: Elsevier

Go, K. S., Son, S. R., & Kim, S. D. (2008). Reaction kinetics of reduction and oxidation of metal oxides for hydrogen production. *International Journal of Hydrogen Energy, 33*(21) doi:10.1016/j.ijhydene.2008.05.039

Hancock, J. D., & Sharp, J. H. (1972). Method of comparing solid-state kinetic data and its application to decomposition of kaolinite, brucite, and Baco3. *Journal of the American Ceramic Society, 55*(2) doi:10.1111/j.1151-2916.1972.tb11213.x

Hossain, M. M., & de lasa, H. I. (2008). Chemical-looping combustion (CLC) for inherent CO2 separations-a review. *Chemical Engineering Science, 63*(18) doi:10.1016/j.ces.2008.05.028

Iliuta, I., Tahoces, R., Patience, G. S., Rifflart, S., & Luck, F. (2010). Chemical-looping combustion process: Kinetics and mathematical modeling. *AICHE Journal, 56*(4) doi:10.1002/aic.11967

IPCC, (2005). *IPCC special report on carbon dioxide capture and storage*, Cambridge, UK: Cambridge University Press

IPCC SPECIAL REPORT ON CARBON DIOXIDE CAPTURE AND STORAGE. (April 01, 2006). *Bulletin of the American Meteorological Society, 87,* 4

Ishida, M., Takeshita, K., Suzuki, K., & Ohba, T. (2005). Application of Fe_2O_3-Al_2O_3 composite particles as solid looping material of the chemical-loop combustor. *Energy & Fuels, 19*(6) doi:10.1021/ef0500944

Ishida, M., Zheng, D., & Akehata, T. (1987). Evaluation of a chemical-looping-combustion power-generation system by graphic exergy analysis. *Energy, 12*(2) doi:10.1016/0360-5442(87)90119-8

Jin, H. G., Okamoto, T., & Ishida, M. (1999). Development of a novel chemical-looping combustion: Synthesis of a solid looping material of $NiO/NiAl_2O_4$. *Industrial & Engineering Chemistry Research, 38*(1) doi:10.1021/ie9803265

Johansson, M. Mattisson, T. Rydén, M. Lyngfelt, A. (2006). Carbon Capture via Chemical-Looping Combustion and Reforming, *International Seminar on Carbon Sequestration and Climate Change*

Johansson, M., T. Mattisson, and A. Lyngfelt.(2006). Comparison of Oxygen Carriers for Chemical-Looping Combustion. *Thermal Science*

Johansson, M., T. Mattisson, and A. Lyngfelt.(2006,21-24 May). Comparison of Oxygen Carriers for Chemical-Looping Combustion of Methane-Rich Fuels. *19th FBC Conference*, Vienna

Lyngfelt, A., Leckner, B., & Mattisson, T. (2001). A fluidized-bed combustion process with inherent CO_2 separation; application of chemical-looping combustion. *Chemical Engineering Science, 56*(10) doi:10.1016/S0009-2509(01)00007-0

Lyngfelt, A. & H. Thunman,(2005). Construction and 100 h of operational experience of a 10-kW chemical-looping combustor. *Carbon Dioxide Capture for Storage in Deep Geologic Formations-Results from the CO_2 Capture Project*. 1: p. 625-645

Mattisson, T., & Lyngfelt, A. (2001 April 18-20). Capture of CO_2 using chemical-looping combustion. *First Biennial Meeting of the Scandinavian-Nordic Section of the Combustion Institute, Göteborg,* pp. 163-168

Mattisson, T., A. Lyngfelt, and P. Cho, (2000, 13-16 August). Possibility of Using Iron oxide as an Oxygen Carrier for Combustion of Methane with removal of CO_2 - Application of Chemical-Looping Combustion. *5th International Conference on Greenhouse Gas Control Technologies*, Cairns, Australia

Moon, I. J., Rhee, C. H., & Min, D. J. (1998). Reduction of hematite compacts by H-2-CO gas mixtures. *Steel Research, 69*(8)

Mukheibir, P., & Ziervogel, G. (2007, 1January). Developing a Municipal Adaptation Plan (MAP) for climate change: the city of Cape Town. *Environment and Urbanization, 19,* 1, 143-158

Nakano, Y., Iwamoto, S., Maeda, T., Ishida, M., & Akehata, T. (1986). Characteristics of reduction and oxidation cyclic process by use of alpha-Fe2o3 medium. *Tetsu to Hagane-Journal of the Iron and Steel Institute of Japan, 72*(10)

Noorman, S., Annaland, M. v. S., & Kuipers, J. A. M. (2010). Experimental validation of packed bed chemical-looping combustion. *Chemical Engineering Science, 65*(1) doi:10.1016/j.ces.2009.02.004

Piotrowski, K., Mondal, K., Lorethova, H., Stonawski, L., Szymanski, T., & Wiltowski, T. (2005). Effect of gas composition on the kinetics of iron oxide reduction in a hydrogen production process. *International Journal of Hydrogen Energy, 30*(15) doi:10.1016/j.ijhydene.2004.10.013

Piotrowski, K., Mondal, K., Wiltowski, T., Dydo, P., & Rizeg, G. (2007). Topochemical approach of kinetics of the reduction of hematite to wustite. *Chemical Engineering Journal, 131*(1-3) doi:10.1016/j.cej.2006.12.024

Richter, H. J., & Knoche, K. F. (1983). Reversibility of combustion processes. *ACS Symposium Series, 235*

Roux, S., A. Bensakhria, and G. Antonini,(2005,10-14 July). Study and comparison of the reactivity of different metallic oxides used as oxygen carriers in the chemical-looping combustion. *World Congress of Chemical Engineering 7th*, Glasgow, United Kingdom. p. 86873/1-86873/9

Sastri, M., Viswanath, R, & Viswanathan, B. (1982). Studies on the reduction of iron-oxide with hydrogen. *International Journal of Hydrogen Energy, 7*(12), 951-955. doi:10.1016/0360-3199(82)90163-X

Scott, S. A., Dennis, J. S., Hayhurst, A. N., & Brown, T. (2006). In situ gasification of a solid fuel and CO2 separation using chemical looping. *AICHE Journal, 52*(9) doi:10.1002/aic.10942

Shimokawabe, M., Furuichi, R., & Ishii, T. (1979). Influence of the preparation history of alpha-Fe2o3 on its reactivity for hydrogen reduction. *Thermochimica Acta, 28*(2), 287-305. doi:10.1016/0040-6031(79)85133-3

Son, S. R., & Kim, S. D. (2006). Chemical-looping combustion with NiO and Fe2O3 in a thermobalance and circulating fluidized bed reactor with double loops. *Industrial & Engineering Chemistry Research, 45*(8) doi:10.1021/ie050919x

Sun, S., & Lu, W. K. (1999). A theoretical investigation of kinetics and mechanisms of iron ore reduction in an ore/coal composite. *ISIJ International, 39*(2) doi:10.2355/isijinternational.39.123

Tiernan, M. J., Barnes, P. A., & Parkes, G. M. B. (2001). Reduction of iron oxide catalysts: The investigation of kinetic parameters using rate perturbation and linear heating thermoanalytical techniques. *Journal of Physical Chemistry B, 105*(1) doi:10.1021/jp0003189+

Toftegaard, M. B., Brix, J., Jensen, P. A., Glarborg, P., & Jensen, A. D. (2010). Oxy-fuel combustion of solid fuels. *Progress in Energy and Combustion Science, 36*(5) doi:10.1016/j.pecs.2010.02.001

Trushens.Sp, Li, K., & Philbroo.Wo. (1974). Nontopochemical reduction of iron oxides. *Metallurgical Transactions, 5*(5) doi:10.1007/BF02644326

Wolf J., (2004). CO_2 Mitigation in Advanced Power Cycles- Chemical Looping Combustion and Steam-Based Gasification, PhD Thesis, Royal Institute of Technology (KTH),Stockholm, Sweden

Zafar, Q., Mattisson, T., & Gevert, B. (2006). Redox investigation of some oxides of transition-state metals Ni, Cu, Fe, and Mn supported on SiO_2 and $MgAl_2O_4$. *Energy & Fuels, 20*(1) doi:10.1021/ef0501389

APPENDIX A EDS Analysis

Table A. EDS Analysis (weight %)

Sample	Fe	O	Al	Mg	Si	Ca	C	Ti	Na	Cr
Iron ore	73.55	22.24	-	0.40	0.70	0.78	2.86	-	-	-
N	55.1	5.083	0.193	0.43	0.95	0.72	37.53	-	-	-
D	56.58	13.28	0.166	0.165	0.91	0.83	28.11	-	-	-
O	42.93	5.1	0.27	0.27	1.06	1.42	49.12	-	-	-
C	71.34	24.6	0.345	0.27	0.89	0.59	2.03	-	0.41	-
D	62.43	30.41	0.26	0.3	0.86	0.49	-	-	-	-
I	60.75	24.29	0.25	0.233	1.12	0.61	11.63	1.48	-	0.55
F	82.50	9.24	0.32	0.235	1.48	1.11	5.4	-	-	-
M	69.68	24.67	0.24	0.315	0.82	0.86	3.61	-	-	-
G	85.89	10.31	-	-	0.86	0.5	2.44	-	-	-
E	61.88	31.02	0.22	0.37	1.365	1.15	5.15	-	-	-
H	66.36	23.93	0.27	0.31	1.3	1.07	6.63	-	0.38	-

Conditions:

Sample N, T=930 ^{0}C, 40ml Ar/20 ml CH_4 , 80 min isothermal, 30 mg.

Sample D, T=950 ^{0}C, 40ml Ar/20 ml CH_4, 80 min isothermal, 20mg.

Sample O, T=945^{0}C, 40ml Ar/20 ml CH_4, 80 min isothermal, 30 mg.

Sample C, T=950 ^{0}C, 100ml Ar/20 ml CH_4, 80 min isothermal, 20 mg.

Sample D, T=950 ^{0}C, 40ml Ar/20 ml CH_4, 80 min isothermal, 20mg.

Sample I, T=930 ^{0}C, 40ml Ar/20 ml CH_4, 80 min isothermal, 30 mg.

Sample F, T=950 ^{0}C, 40ml Ar/20 ml CH_4, 70 min isothermal, 60 mg.

Sample M, T=930 ^{0}C, 30ml Ar/20 ml CH_4, 20 min isothermal, 30 mg.

Sample G, T=950 ^{0}C, 40ml Ar/20 ml CH_4, 80 min isothermal, 30 mg.

Sample E, T=950 ^{0}C, 40ml Ar/20 ml CH_4,15 min isothermal,20 mg.

Sample H, T=910 ^{0}C, 40ml Ar/20 ml CH_4, 80 min isothermal, 30 mg.

APPENDIX B SEM Images

Sample **C**, T=950 ^{0}C, 100ml Ar/20 ml CH_4, 80 min isothermal, 20 mg	Sample **E**, T=950 ^{0}C, 40ml Ar/20 ml CH_4, 15 min isothermal ,20 mg
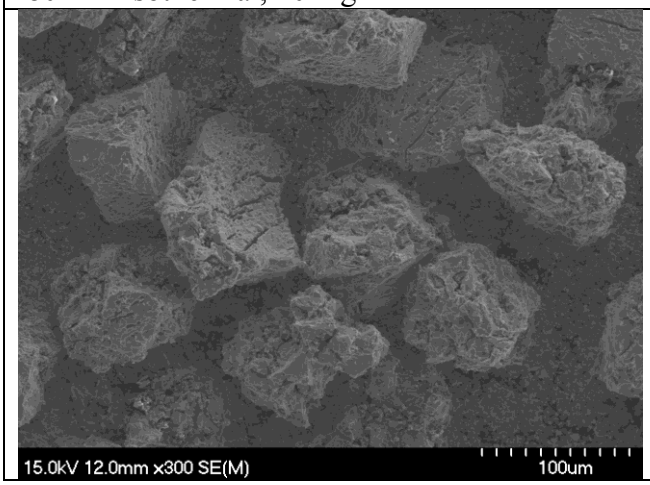	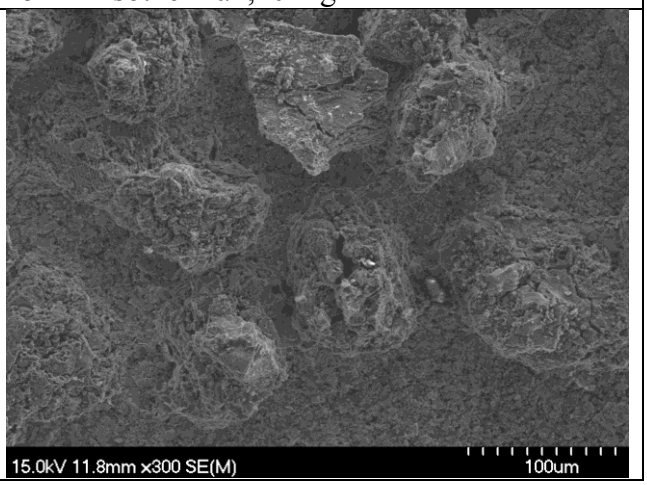

Figure B1.The SEM images of sample C and E, 300 x magnifications.

Sample **D,** T=950 ^{0}C, 40ml Ar/20 ml CH_4, 80 min isothermal, 20mg	Sample **H**, T=910 ^{0}C, 40ml Ar/20 ml CH_4, 80 min isothermal, 30 mg
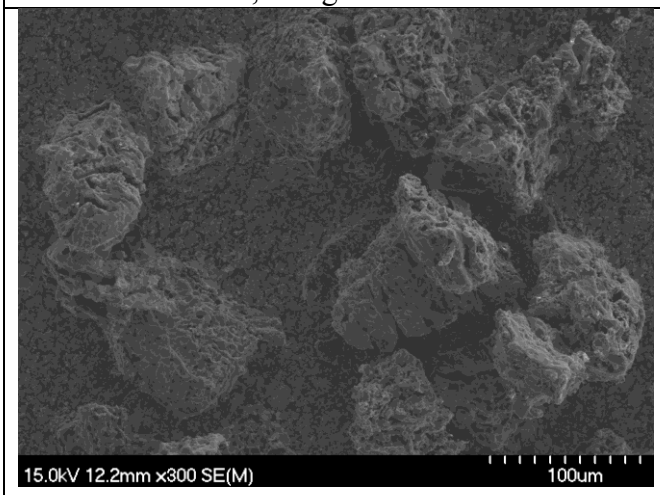	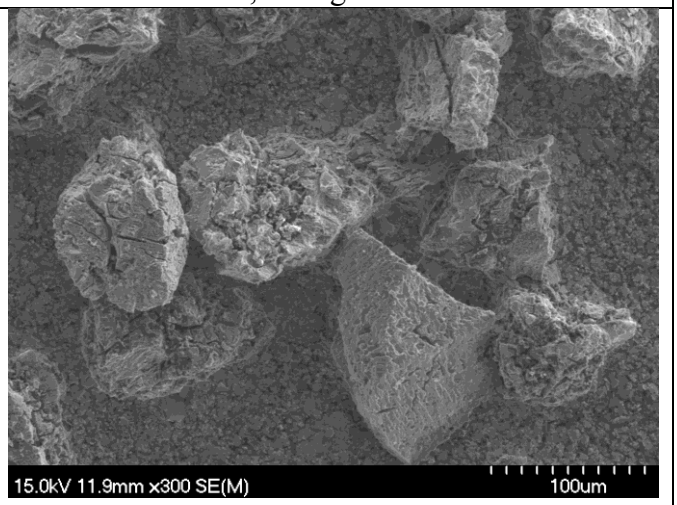

Figure B2.The SEM images of sample D and H, 300 x magnifications.

Sample **G**, T=950 ^{0}C, 40ml Ar/20 ml CH_4, 80 min isothermal, 30 mg	Sample **F**, T=950 ^{0}C, 40ml Ar/20 ml CH_4, 70 min isothermal, 60 mg
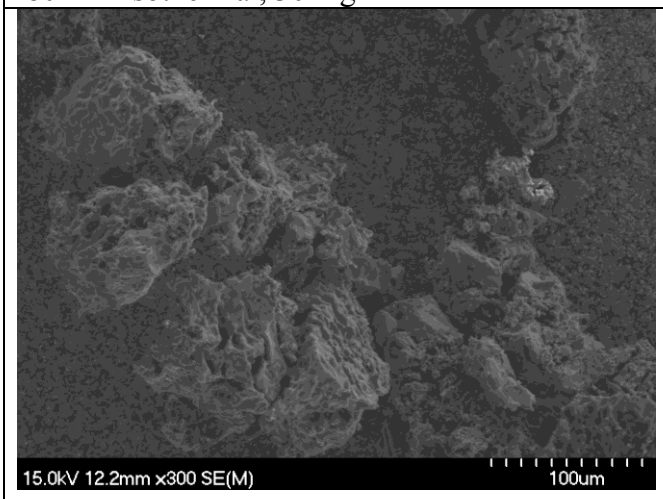	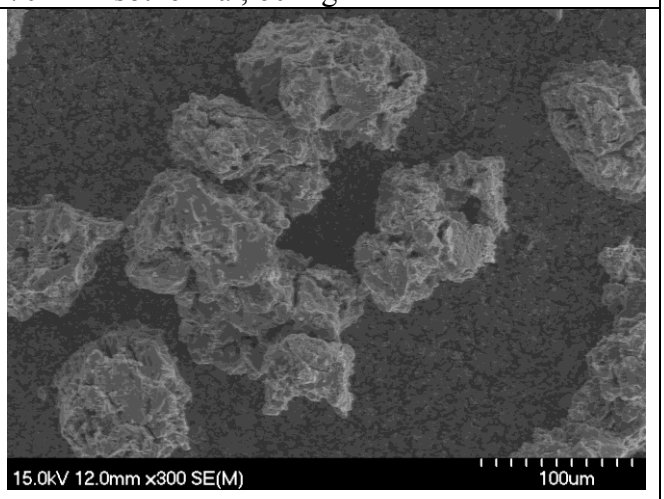

Figure B3.The SEM images of sample G and F, 300 x magnifications.

Sample **M** , T=930^{0}C, 30ml Ar/20ml CH_4, 20 min isothermal, 30 mg	Sample **N**, T=930 ^{0}C, 40ml Ar/20 ml CH_4, 80 min isothermal, 30 mg
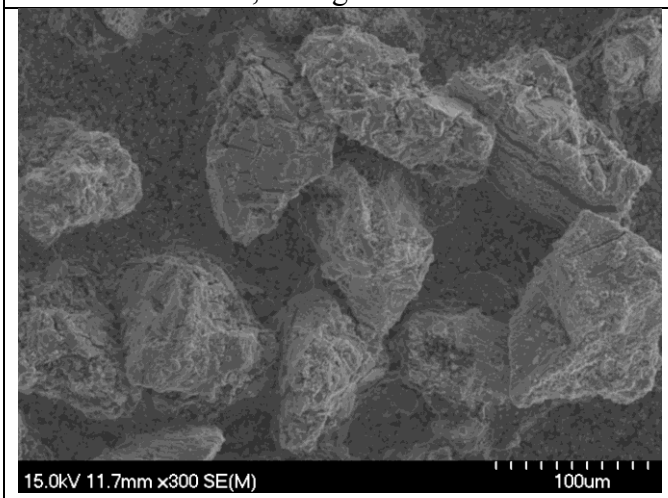	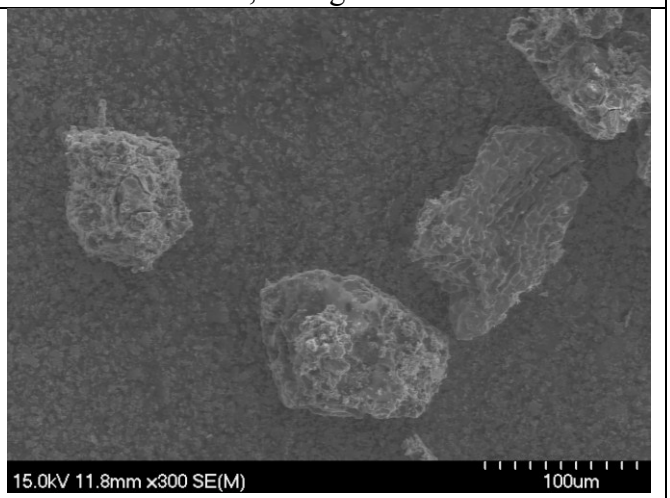

Figure B4.The SEM images of sample M and N, 300 x magnifications.

Sample **I** , T=930 ^{0}C, 40ml Ar/20 ml CH_4, 80 min isothermal, 30 mg	Sample **O** , T=945 ^{0}C, 40ml Ar/20 ml CH_4, 80 min isothermal, 30 mg
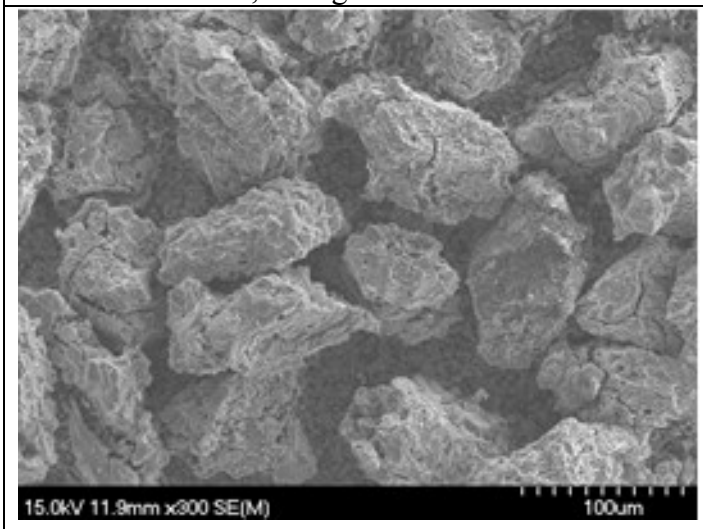	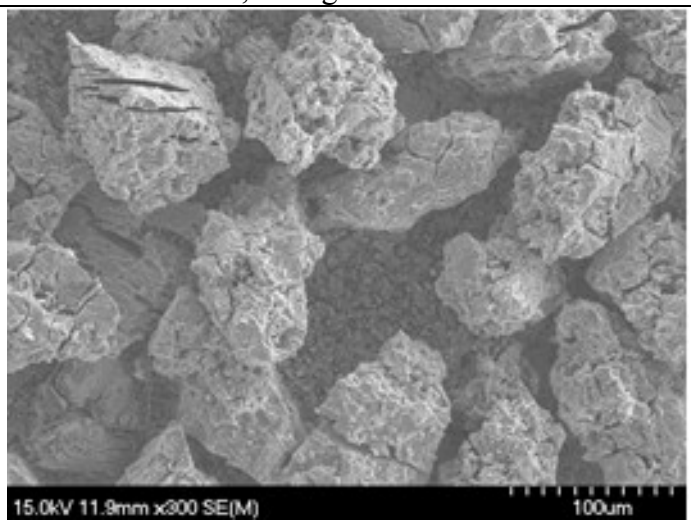

Figure B5.The SEM images of sample I and O, 300 x magnifications.

Appendix C Experimental graphs Obtained From the Thermogravimetric Analyzer

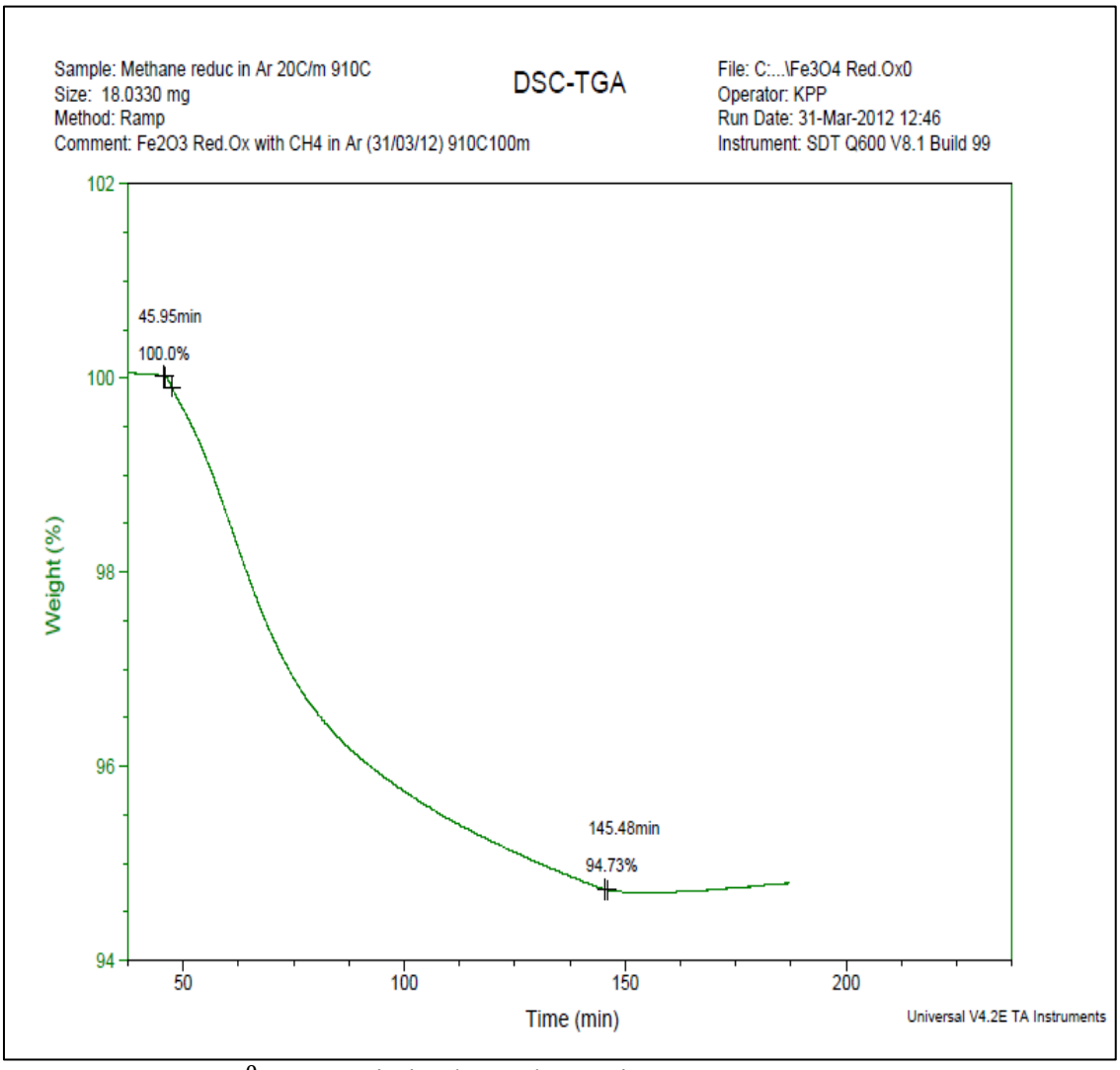

Figure C1. T=910 ^{0}C, 100 min isothermal experiment,100 Ar:20 CH_4.

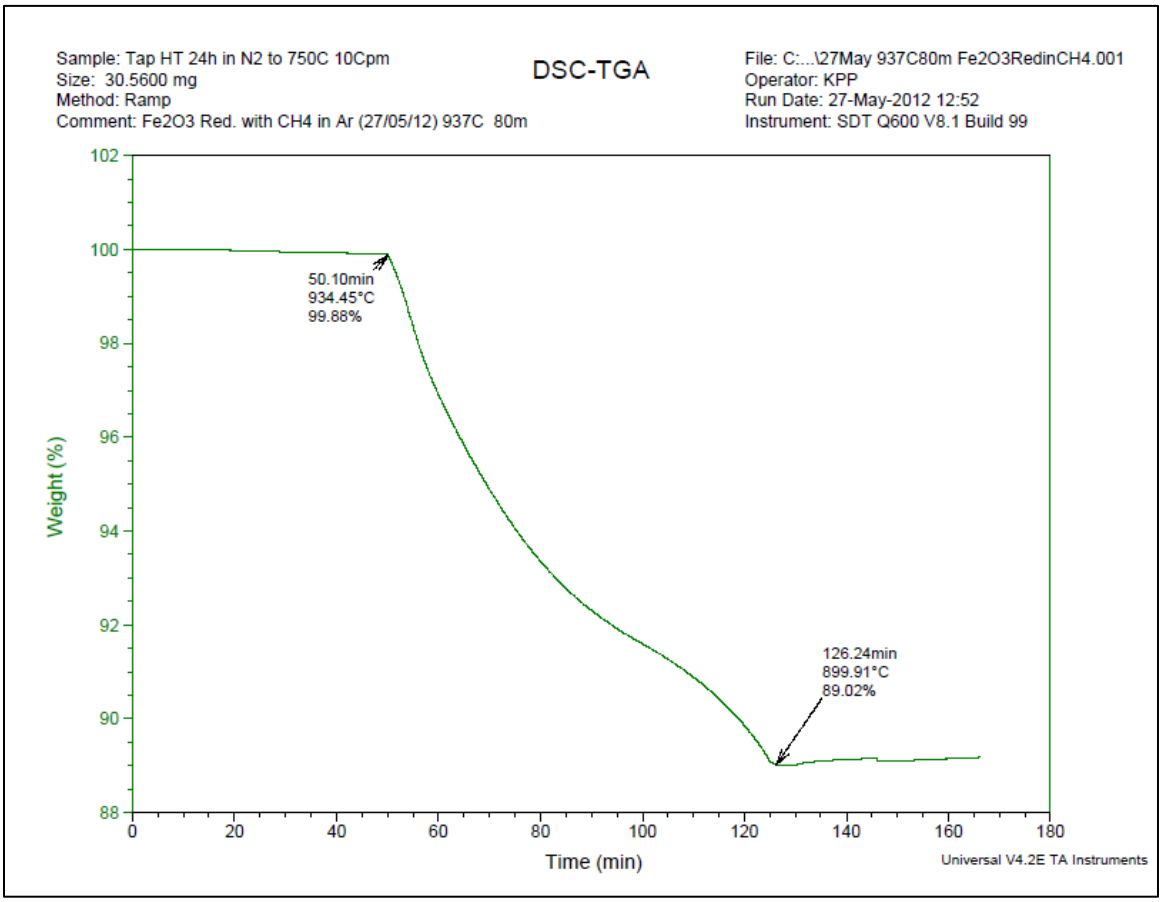

Figure C2. T=937 ^{0}C, 80 min isothermal experiment, 30 Ar: 20 CH_4.

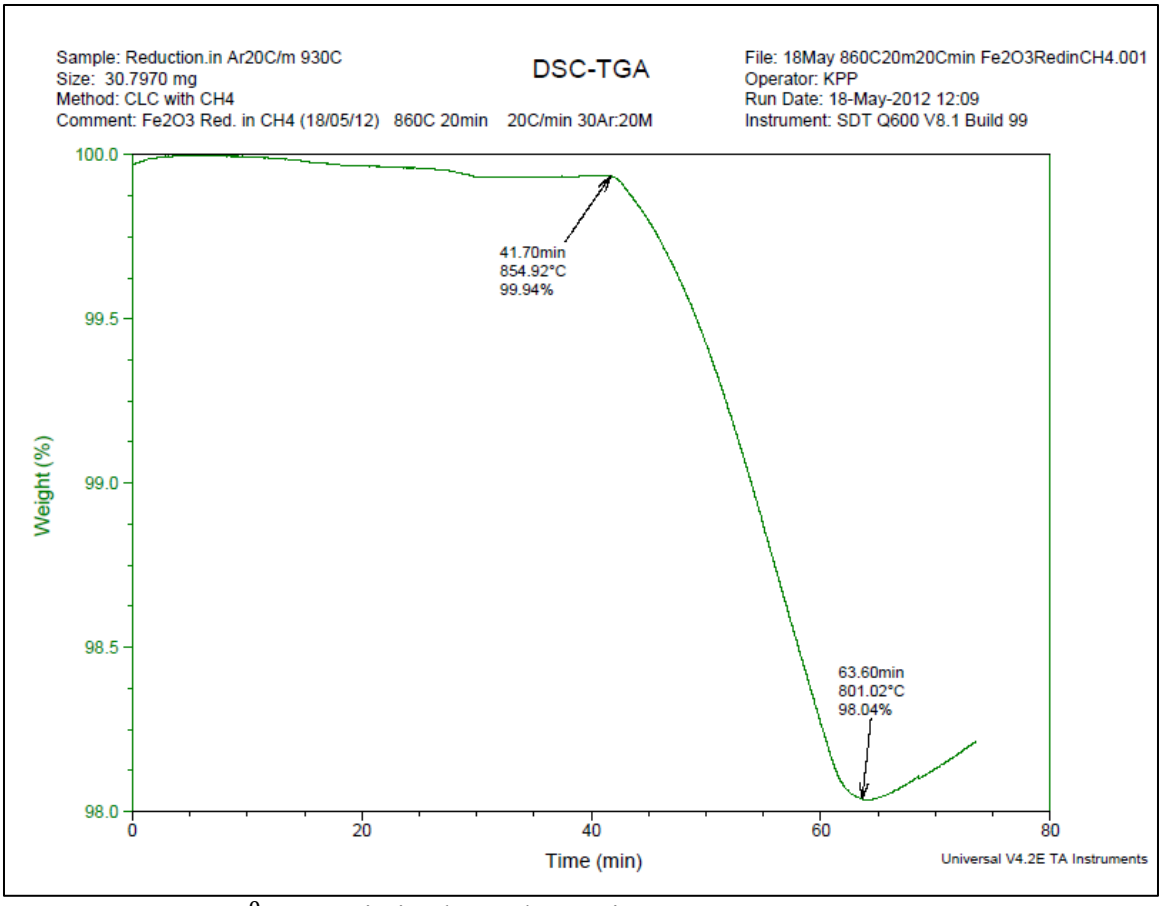

Figure C3. T=860 ^{0}C, 20 min isothermal experiment, 30 Ar: 20 CH_4.

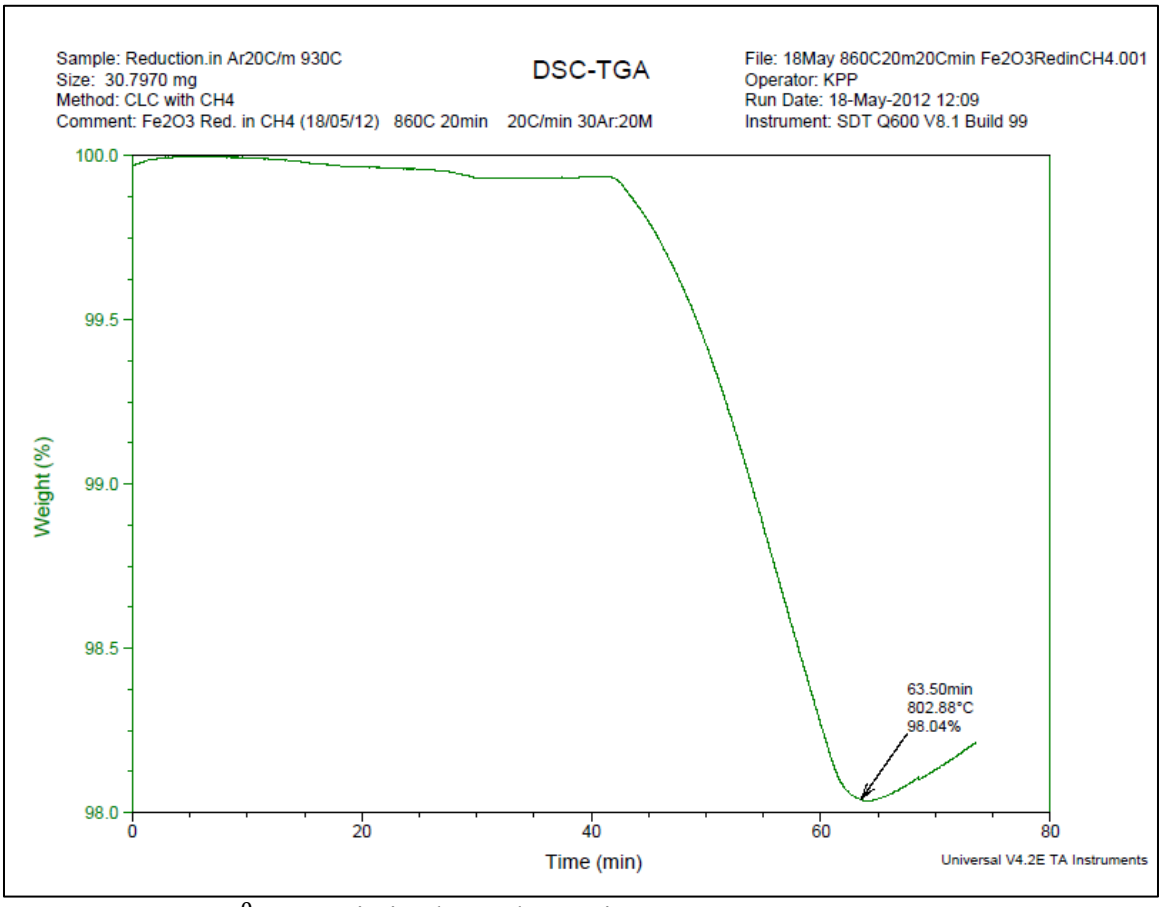

Figure C4 T=860 ^{0}C, 20 min isothermal experiment, 30 Ar: 20 CH_4.

Appendix D Conversion Time Plots

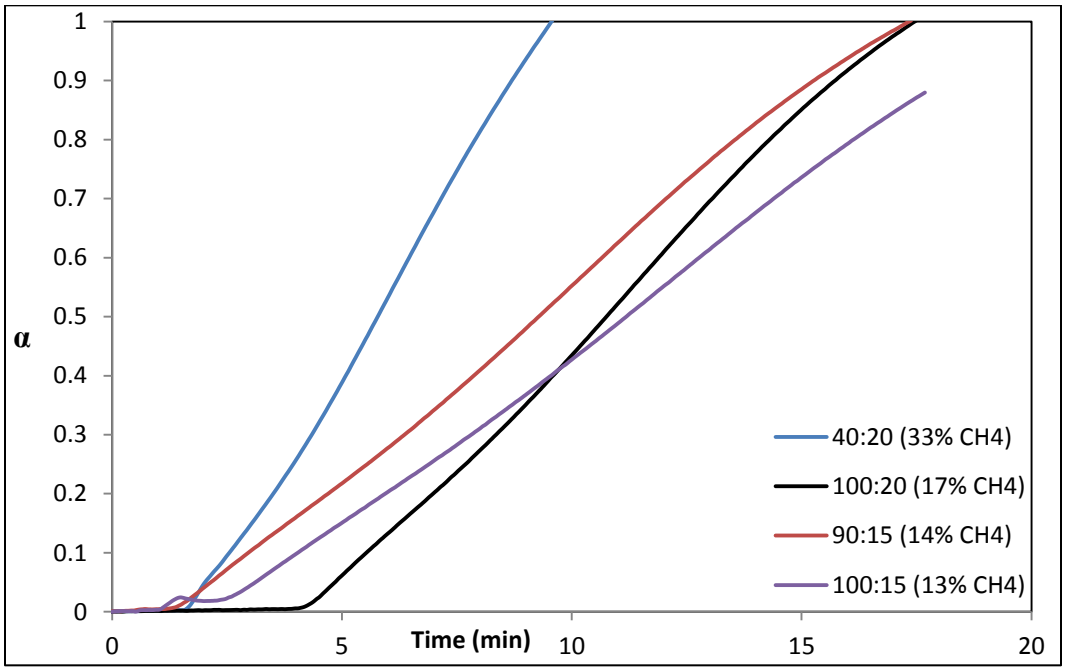

Figure D1. Coneversion-time plot, CH_4 flow varaition.

Appendix E XRD RESULT

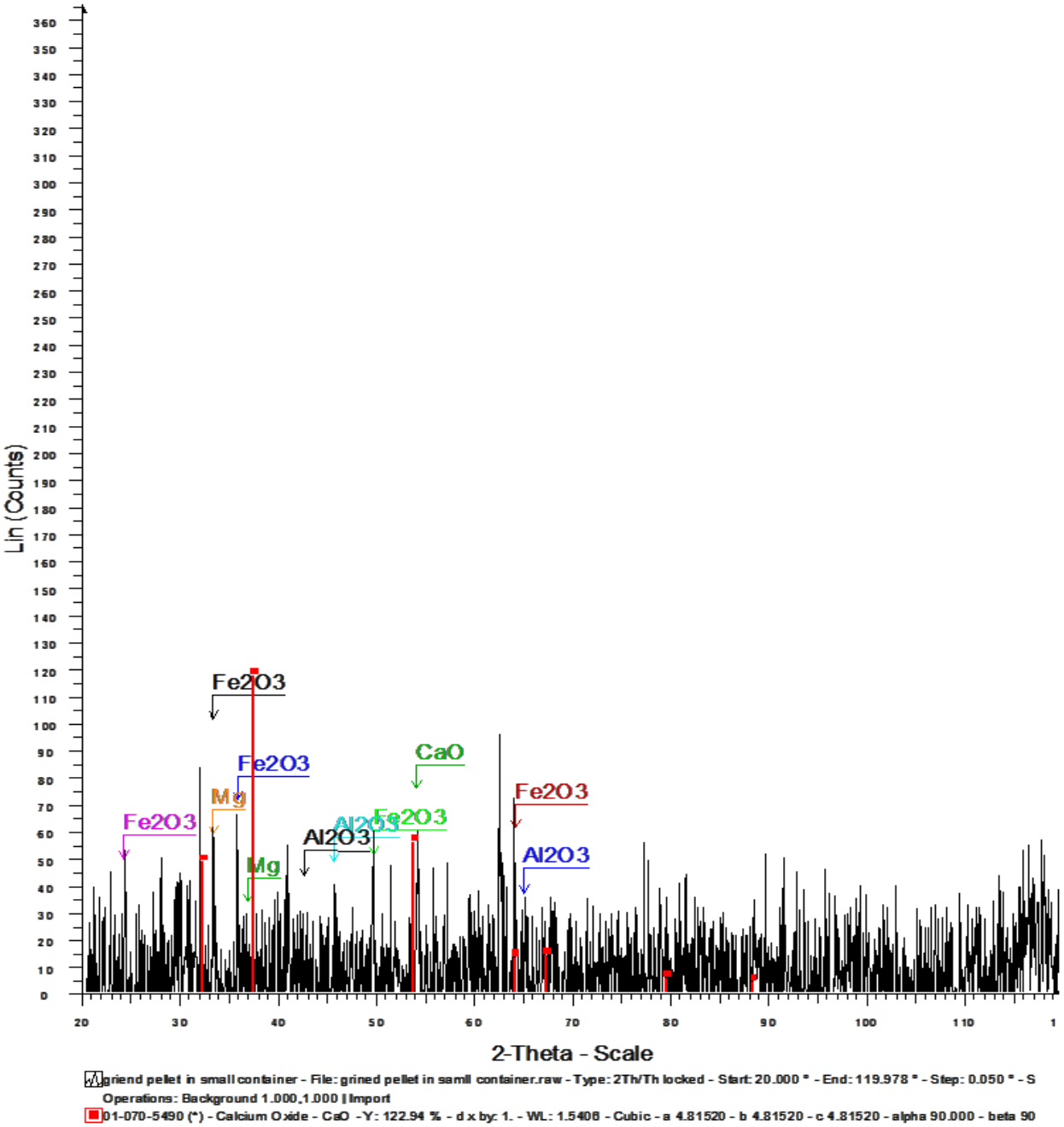

Figure E1. XRD result of iron ore.

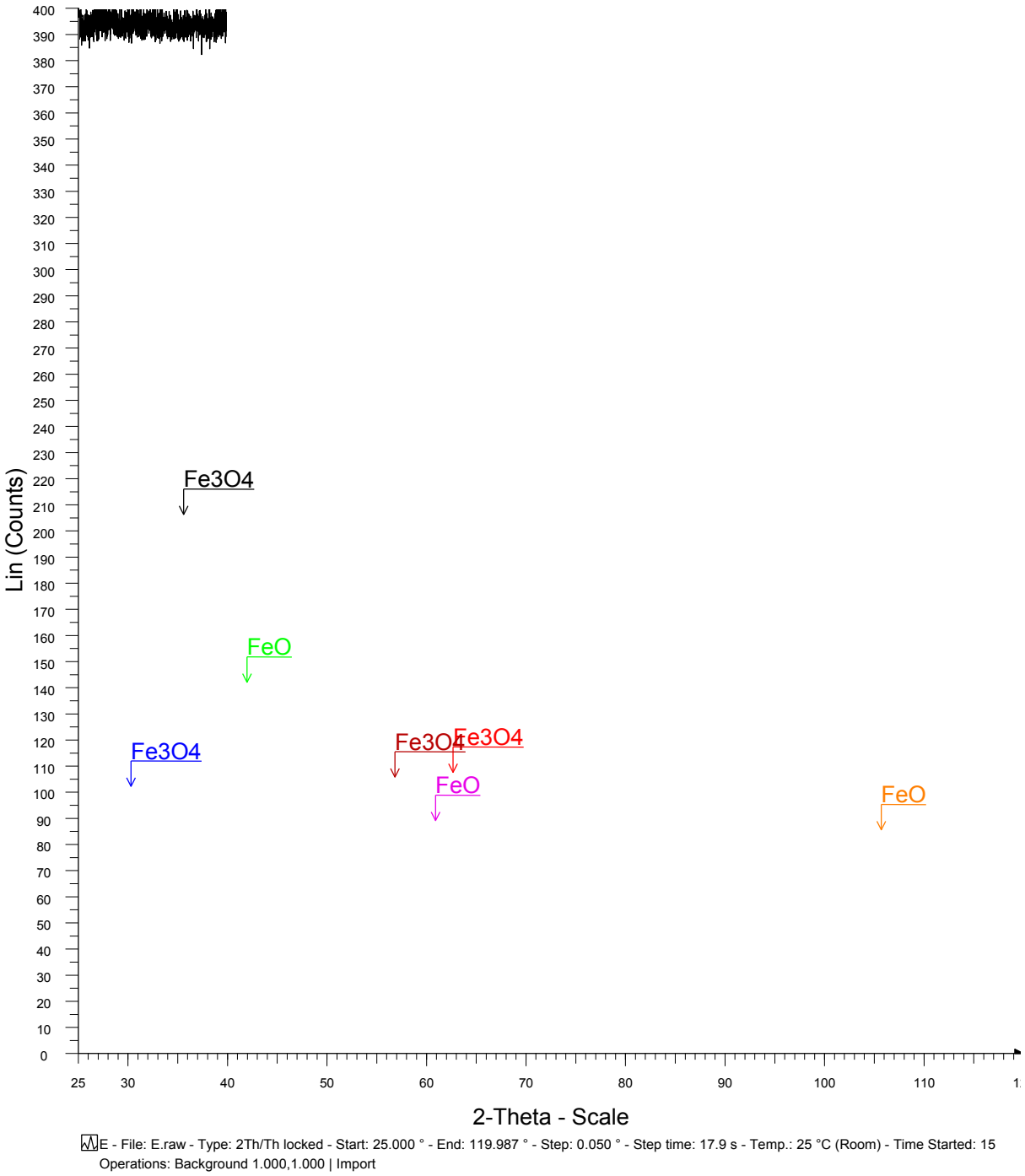

Figure E2. XRD result of a 20 min isothermal , 30Ar:20 CH_4.

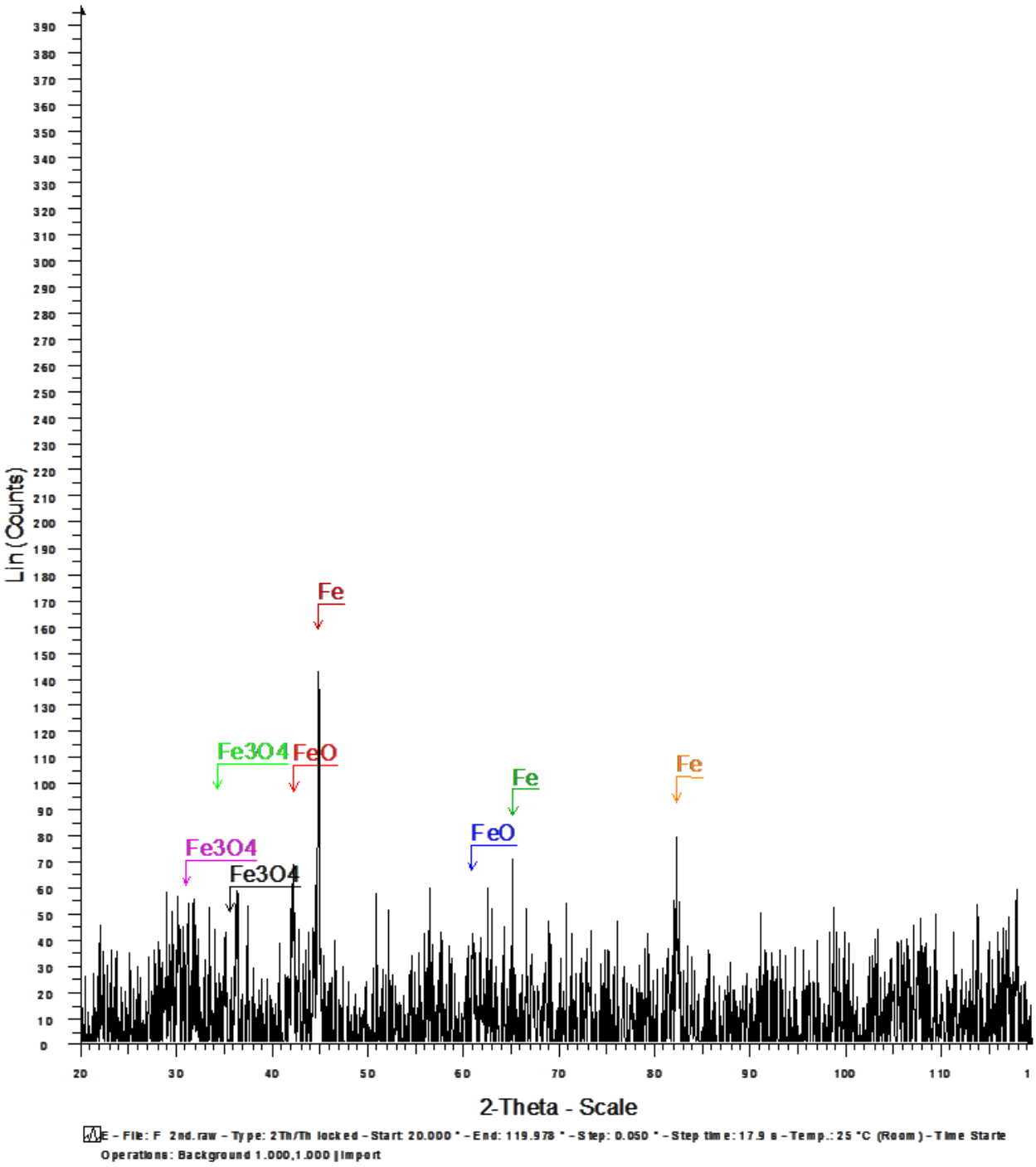

Figure E3. XRD result of a 60 min isothermal , 30Ar:20 CH_4.